Thesis

Quantum Single-Particle Generator and Shot Noise in Mesoscopic Systems

Eiki Iyoda
Department of Physics, University of Tokyo
December, 2011

Abstract

In this thesis, we study quantum nature of mobile quantum objects through the setup of the Hong-Ou-Mandel-type experiment, which reflects statistical properties of the objects. We first study effect of environmental noise in solid state devices for single-photon generation. We derive density matrix of emitted photons in a fully analytic form, and calculate survival probabilities, spectra, and purities of emitted photons under pure dephasing induced by energy level fluctuation. We discuss what extent quality of quantum coherence of emitted photons is affected by noise, and how it is improved by time filtering. We also study effect of environmental noise and Coulomb interaction on single-electron generation using a chiral edge state in integer quantum Hall effect. We discuss how noise and the Fermi-edge singularity of edge states affect quantum coherence of emitted electrons. These results will provide a useful aspect on future application on quantum information technology using mobile quantum objects. Finally, we calculate finite-temperature noise due to fractional charge excitations in order to access fractional statistical properties of quasiparticles. We propose an extended shot noise calculated from experimentally available data, and demonstrate that it is useful to determine the statistical angle of quasiparticles.

This is a version, which is uploaded on the Web. Figures taken from previous studies are omitted.

Acknowledgments

I am sincerely grateful to Prof. Takeo Kato for continuous discussions and tolerance encouragement throughout my graduate course. I would also like to thank Prof. Kazuki Koshino for stimulating discussions. I wish to acknowledge to Tatsuya Fujii for powerful discussions. I am grateful to Prof. Yasuhiro Utsumi and Prof. Kensuke Kobayashi who give me many chance to think about mesoscopic physics. I thanks to Prof. Takao Aoki and Prof. Keiichi Edamatsu for a joint research. I am deeply grateful to Ken-Ichiro Imura and Hideaki Maebashi for their hearty encouragement. I thank to all the people who spend invaluable time together at physics meetings, workshops, and summer schools. I would like to thank my colleagues of Institute for Solid State Physics, University of Tokyo. Especially, Shunsuke Furuya, Shintaro Takayoshi, Yasuo Ohta, Kouhei Ohnishi, Shun Maruyama, Ryo Tamura and the member of Kato group, Kazuyoshi Yoshimi, Hiroshi Shinaoka, Yuji Hamamoto, Itofumi Takeuchi, Noritaka Tamura, Hiroyuki Abe, and Shigeru Sumi for daily discussion and conversation. I am indebted to Hiroko Eguchi who enabled me to live a good laboratory life.

Finally, I acknowledge my family for heartful encouragement and financial supports. I also acknowledge the financial support by GCOE for Phys. Sci. Frontier, MEXT.

Contents

Chapter 1

Introduction

In this chapter, we overview the background of the present research, and present the purpose of this thesis. A detailed review of previous experimental and theoretical studies related to this thesis is given in Chap. 2.

1.1 Overview

Coherent control of quantum states in physical systems is now of much importance in various research fields. Quantum manipulation of quantum states not only provides appealing demonstration on the foundation of quantum mechanics such as examination of breaking of Bell's inequality, but also gives a vital building block of quantum information technology (quantum communication, quantum computation, etc.) [1]. In a number of early studies, quantum manipulation was tried to spatially-fixed objects such as ions trapped by laser, cavity-QED systems, Josephson devices, quantum dots, and so on. Recently, mobile quantum objects have been attracting much interest, because they are expected to play an important role in quantum information transfer between spatially-fixed quantum objects. Mobile quantum objects are also useful in experimental demonstration of 'non-locality' in quantum mechanics as nonlocal correlation between spatially-separate quantum objects is easily generated.

Realization of mobile quantum objects has been considered so far in two kinds of particles, bosons and fermions. Let us first discuss the first type of particles, i.e., bosons. The most famous object of this kind is a photon. Quantum nature of photons has been of a central topic for a few decades in the research field called 'quantum optics' [2, 3]. Technology of quantum optics is being developed even now, and has enable us to manipulate a quantum state of a single photon, to entangle a few photons, and to utilize photons for quantum communication. In spite of these successes, there are a disadvantage in use of photons as mobile quantum objects; interaction between photons is usually weak. To increase interaction between photons, one may consider use of excellent nonlinear optical materials. Another promising way is to employ a combined system of a single atom and a cavity, which is called a cavity quantum electrodynamics (cavity QED) system [4, 5]. This system can naturally introduce strong interaction between photons through nonlinearity of the system prohibiting an atom to be excited twice. Further recent progress in quantum optics enables us to fabricate a novel type of the cavity QED system composed by an optical cavity and a quantum dot, both of which is made in semiconductors [6]. The semiconductor cavity QED has an advantage that an atomic system (a quantum dot) is spatially fixed and can couple cavity photons continuously, in contrast with the original cavity QED system where atoms stay in a cavity with a finite dwell time. The semiconductor cavity QED is now considered to be a promising candidate for quantum information processing with photons in solid state devices. The cavity QED system in solid state devices provides a novel feature originating from strong influence of the environment. The atomic level is no longer isolated, and couples to the background fluctuation. This environment effect induces new effects as discussed in Sec. 2.1.

The second type of mobile quantum objects are fermions. The most famous object following fermi statistics is, of course, an electron. In contrast with photons, quantum control of *mobile* electrons started only several years ago. For generation of nonlocal quantum correlation, one-dimensional electron systems have frequently been considered theoretically. A chiral edge state in the integer quantum Hall (IQH) states [7] is a good candidate for a quantum propagation of electrons, since backward scattering by impurities and potential inhomogeneity is well suppressed. Actually in 2007, a single-electron injection from a quantum dot into an edge state has been realized experimentally by using a rapid temporal change of a gate voltage [79]. This result reminds us of a fermionic analogy of experiments in quantum optics if an edge state and a tunneling junction of edge states are considered to be a light-propagating channel and a half-mirror. This experiment opens up a possibility of a novel quantum device using mobile quantum objects. For actual application, we should note that electrons in chiral-edge channels system may suffer strong perturbation from an (electronic) environment because of the Coulomb interaction. The coupling between electrons and an environment induces pure dephasing, and affects quality of quantum information carried by propagating electrons in edge channels. (Detailed review is given in Sec. 2.2.)

The most remarkable difference between photons and electrons is the change of the wave function in exchanging indistinguishable particles; the sign of the wave function is invariant in exchanging bosons (like photons), whereas it is changed in exchanging fermions (like electrons). This difference is strikingly observed in the so-called Hong-Ou-Mandel experiment [9]), which is a variant of the Hanbury Brown-Twiss experiment [10, 11, 12, 13, 14, 15]. We show a schematic setup of the Hong-Ou-Mandel experiment in Fig. 1.1 (a), where two input particles simultaneously enter a half mirror M from a channel 1 and 2, and scatter out into a channel 3 or 4. If the particles are bosons, both of two particles always scatter out into the same channel, i.e., both go into the channel 3 with a probability 1/2 and into the channel 4 with a probability 1/2. On the other hand, if the particles are fermions, each of them always scatters out respectively into the different channels, i.e., one of two goes into the channel 3 and the other into the channel 4. In other words, the coincidence probability P_{34} that one of two particles goes out into the channel 3 and the other into the channel 4 is 0 for bosons, and 1 for fermions. The fermionic analogy of the Hong-Ou-Mandel experiment is actually

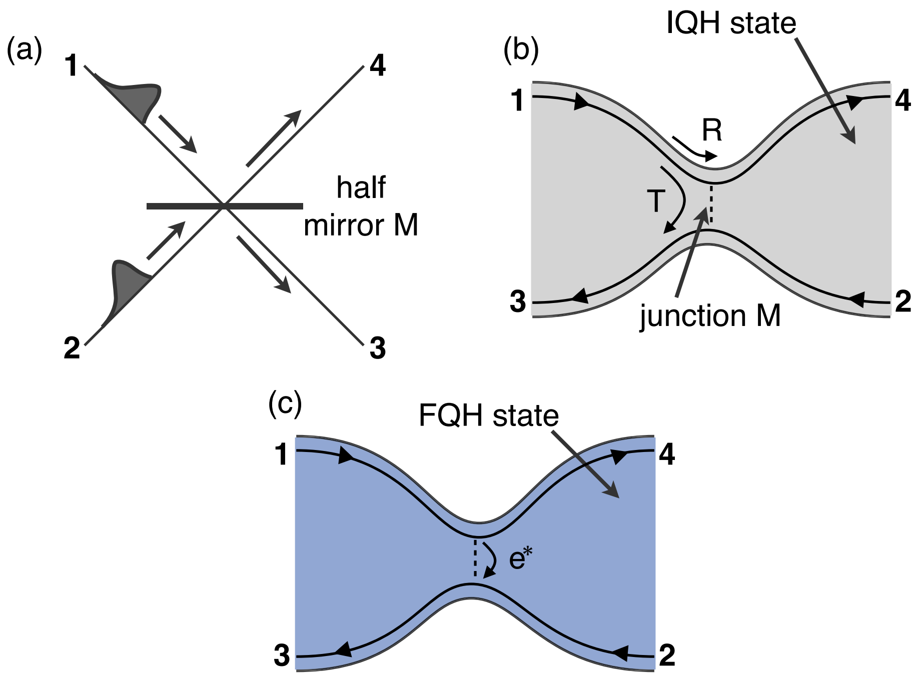

Figure 1.1: Schematic illustrations of systems treated in this thesis. (a) Hong-Ou-Mandel interference experiment (b) two chiral edge channels in IQH, coupled to each other at a junction M (c) two chiral edge channels in FQH. quasi-particle with charge e^* tunnels at a junction M

realized in the IQH edge states as shown in Fig. 1.1 (b). Here, two chiral edge channels are coupled to each other at a junction M. We assume that when one electron in channel 1 enters the junction M, it go through the junction into the channel 3 with a probability T, and tunnels(reflects) into the channel 4 with a probability R. Similarly, we assume that if one electron in channel 2 enters the junction M, it go through the junction into the channel 4 with a probability T, or tunnels into the channel 3 with a probability R. For the half-mirror condition $T = R = 1/2$, the system shown in Fig. 1.1 (b) provides an analogy of the fermionic Hong-Ou-Mandel experiment. Although several experimental groups have now been trying to realize this type of experiments by using a single-electron generator in semiconductors, its experimental demonstration has not been reported so far.

In this thesis, we point out that the Hong-Ou-Mandel experiment can be utilized for evaluation of quality of quantum information carried by mobile quantum objects. Actually, as shown in Sec. **??**, the coincidence probability P_{34} is related to the purity of one incident particle state as $P_{34} = 1 \mp \mathcal{P}$ where $-(+)$ is for bosons(fermions). Here, the purity $\mathcal{P} = \mathrm{Tr}\rho^2$ is a measure of how the wave function of the incident particle retains quantum coherence, and takes 1 and 0 for a pure state and a fully mixed state, respectively. Thus, the coincide probability in the Hong-Ou-Mandel experiment gives a direct measure of quantum coherence of a single particle. One of the main subjects in this thesis is to study how dephasing process in a single particle generator made in solid state devices affects coherence of quantum mobile objects by evaluating the coincide probability in the Hong-Ou-Mandel experiment setup.

In condensed matter physics, it is known that there exists the third type of mobile quantum objects called an anyon. Anyons are described as elementally quasi-particle excitations in the fractional quantum Hall (FQH) effect [16, 17]. Although precise theoretical description on statistics in exchanging two anyons is difficult in general, simple argument is possible for some special cases. We show one example in Fig. 1.1 (c), where the setup is almost the same as Fig. 1.1 (b) except for replacing the region between two edge channels from the IQH state to the FQH state. When we take the reflection probability R as small ($R = 1 - T \ll 1$), the fundamental charge-transfer process at the junction is dominated by one quasi-particle excitation in FQH states with a fractional charge e^* The fractional charge e^* is equal to νe in Laughlin state, where ν is a filling factor. Then, the effective charge e^* can be observed by measurement of shot noise, i.e., partition noise at the junction [18, 19, 20, 21]. Statistics of anyons, however, is not characterized by an effective charge e^*, but by a statistical angle θ defined by the extended commutation relation $c_i c_j^\dagger - e^{i\theta} c_j^\dagger c_i = \delta_{ij}$. Whereas the statistical angle of anyons in FQH states is given simply by $\theta = \nu\pi$ for the Laughlin states $\nu = 1/(2n + 1)$, it takes more complex values in general hierarchical FQH states, and is in general independent of the effective charges e^*. The statistical angle has been studied experimentally by the Aharonov-Bohm oscillation in a ring fabricated by FQH edge states [22]. However, direct observation of anyons statistics in two-particle exchange process such as the Hong-Ou-Mandel-type experiment still remains a challenge.

1.2 Purpose of this thesis

In this thesis, we theoretically study the following three subjects, all of which are closely related to statistics of mobile quantum objects.

1.2.1 Single photon generator (Chap. 3)

We study a quantum nature of a single photon generated from a cavity QED system in semiconductors [23]. We consider dephasing effect due to white-noise energy-level fluctuation in a quantum dot by introducing an additional one-dimensional bosonic port. We show that all the quantities of interest on a generated photon can be calculated analytically in this simplified model. We show that novel features on quantum coherence of a generated photon in solid state devices are obtained through calculation of a survival probability, a spectrum, and a purity despite simpleness of the model.

1.2.2 Single electron generator (Chap. 4)

We study a quantum nature of a single electron generated from a quantum dot into an IQH edge channel. As source of dephasing on electrons, we consider (1) white-noise energy level fluctuation in a quantum dot and (2) (screened) Coulomb interaction between an electron in a dot and electrons in a edge channel. We calculate a survival probability, a spectrum, and a purity in this system. In particular, we show that Coulomb interaction induces the so-called 'fermi-edge singularity' effect, and strongly affects coherence of a generated electron.

1.2.3 Shot noise in FQH edge states (Chap. 5)

We study current noise at finite temperatures under weak reflection between two FQH edge states [24]. We define an (extended) Fano factor at finite temperatures, which can be obtained from measurement of noise power and nonlinear differential conductance. We show that this extended Fano factor is useful to experimentally detect a statistical angle. We demonstrate that the extended Fano factors show different behaviors for $\nu = 1/5$ and $\nu = 2/5$ even though the fractional charge is given by $e^*/5$ for both FQH states.

Chapter 2

Review

In this chapter, we present a detailed review on single-particle generation. We describe previous experimental and theoretical works on individual topics, single-photon generation (Sec. 2.1), single-electron generation (Sec. 2.2), fractional charge excitation and shot noise in FQH edge states (Sec. 2.3).

2.1 Single Photon Generation

2.1.1 Cavity QED systems

As mentioned in Chap. 1, a key factor in future development of quantum optics is control of strong nonlinear coupling between photons. One hopeful candidate is a cavity QED system [4]. Fig. 2.1 shows a schematic figure of a typical cavity QED setup. Two mirrors located in an extreme high vacuum constitute a high-Q cavity for a photon frequency ω_c. One of two mirrors has weak photon leakage, whose rate is denoted with κ, into an output light channel connected to a photon counter. One atom flows slowly through the cavity, and stays in the cavity in a finite dwell time. Atoms in the cavity can interact with the photon field through a dipole interaction. For simplicity, an atom is assumed to have only two quantum levels with an energy difference ω_a, and its coupling to the cavity fields to be a constant g independent of the photon frequency

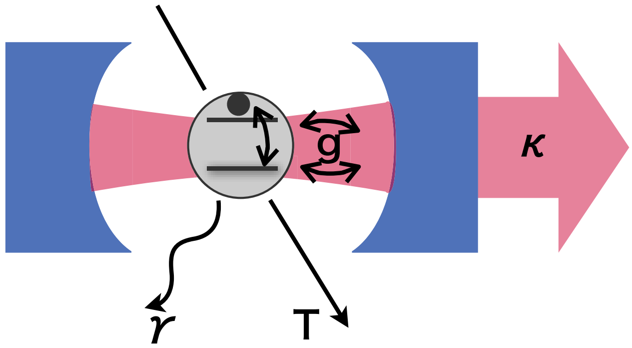

Figure 2.1: Characteristic setup of the cavity QED system, composed of an atom, a cavity, and an environment (an output channel).

ω around the cavity frequency ω_c. Then, the system Hamiltonian is described within the rotating wave approximation as

$$H_0 = \omega_a \sigma^\dagger \sigma + \omega_c a^\dagger a + g(\sigma^\dagger a + a^\dagger \sigma), \tag{2.1}$$

where $a(a^\dagger)$ is an annihilation(a creation) operator of the cavity photon field, and σ is a transition operator of the atom. This model is known as the Jaynes-Cummings model [25, 26]. There are several methods to add leakage effect into an output channel. The simplest method to describe it in a fully quantum mechanical way is to introduce a one-dimensional bosonic port [27, 28, 29, 30], whose Hamiltonian is given as

$$H_{\mathrm{leak}} = \int k b_k^\dagger b_k \mathrm{d}k + \sqrt{\frac{\kappa}{2\pi}} \int \mathrm{d}k (b_k^\dagger a + a^\dagger b_k). \tag{2.2}$$

The cavity QED system has an important feature useful for quantum manipulation of photons. Let us first consider the Jaynes-Cummings Hamiltonian H_0 for the nearly tuned case ($\omega_a \sim \omega_c$) in the space spanned by two state bases; one is a state of an excited atom plus no cavity photon, and the other is of a ground-state atom plus one cavity photon. These two states are mixed by the atom-cavity coupling g, and the eigenenergy of H_0 is given as $E = \bar{\omega} \pm \sqrt{(\delta\omega)^2 + g^2}$, where $\bar{\omega} = (\omega_a + \omega_c)/2$ and $\delta\omega = (\omega_c - \omega_a)$. For the perfectly tuned case ($\delta\omega = 0$), the energy splitting is $2g$, which is called the vacuum Rabi coupling. By a similar way, the energy splitting

Figure 2.2: Three types of optical cavities in semiconductors. (a) A photonic-crystal-slab nanocavity, (b) a micropillar, and (c) a microdisk. (Cited from [6].)

between high-energy states, a N-photon plus excited-atom state and a $N+1$-photon plus ground-state-atom state is calculated as $2g\sqrt{N+1}$. Clearly, the photon fields yields nonlinearity with respect to the cavity photon intensity N by the presence of atoms. This nonlinearity of photon fields is useful for nonlinear optics such as laser physics [6]. Even in linear optics, the cavity QED system is useful in quantum manipulation of photons and atomic states. For actual use of the cavity QED, it is required to increase the vacuum Rabi coupling g. Although the coupling g was usually smaller than κ in early studies of the cavity QED, it has been increased in recent experiments close to (or in some case larger than) κ. We call the former condition $g < \kappa$ as weak coupling and the latter $g > \kappa$ as strong coupling. In the strong coupling condition $g > \kappa$, an appropriately prepared initial state can oscillate in the Hilbert space spanned by two states (N photon plus excited atom and $N+1$ photon plus ground-state atom) with a frequency $2g\sqrt{N+1}$. This is called the vacuum Rabi oscillation.

For single photon generation, we may naively expect that large coupling strength g is favorable since rapid emission of photons into the cavity can be realized. The best condition for single photon generation is, however, nontrivial. One reason is that for large values of g photon emission into an output channel is bottlenecked by leakage rate κ. Another reason is that environment effect such as unintended emission into vacuum. For example, single photon generation by using π-pulse excitation of an atom has been studied theoretically [31, 32].

2.1.2 Cavity QED systems in solid state devices

Rapid development of nanoscale fabrication technique has now enabled to realize a cavity QED system in solid state devices. Weak Rabi-vacuum coupling between a semiconductor quantum dot and a cavity photon field as well as its application to single photon generation has already been realized a decade ago [33, 34, 35, 36, 37]. Realization and control of strong Rabi-vacuum coupling are now one of hot topics in quantum optics in semiconductors [6], since they are useful for creating compact optical devices. There are several ways for fabrication of cavities to realize a large vacuum Rabi splitting. In Fig. 2.2, we summarized three types of optical cavities, a photonic-crystal-slab nanocavity [38], a micropiller [39], and a microdisk [40]. Though there are advantages and disadvantages for each of these types of cavities, the cavity frequency, the leakage frequency, and Rabi vacuum coupling in these systems are roughly given as $\omega_c \simeq 3-5\times10^5$GHz, $\kappa \simeq 40$GHz, and $g \simeq 40-200$GHz, respectively [39, 38, 40]. This strong-coupling cavity-dot system has been utilized to fabricate a single-dot laser [41] and to generate nonclassical light [42, 43].

Another important physical system for realization in cavity QED in solid state devices is a superconductoring device [44]. After the first experimental realization [45], there have appeared a number of remarkable experimental results including generation of single microwave photons [46], generation of Fock states [47], and tomography of arbitrary states between a qubit and a cavity field [48]. We, however, will not discuss experimental relevance of this thesis to the superconducting cavity QED, because environment noise in this system is governed by low frequency $1/f$ noise [49], which is difficult to be treated in the method adopted in this thesis based on white noise. Although we should keep in mind importance of dephasing problem in the superconducting cavity QED, we will left it as a future problem here.

Figure 2.3: (a) A photoluminescence spectra of a photonic-crystal-slab cavity coupled to a quantum dot. Each curve is obtained by changing Xe pressure, which condensate on a semiconductor surface. (b) Change of peak positions. (Cited from [50].)

2.1.3 Dephasing effect in cavity QED systems

Single photon generator made by the cavity QED system in solid state devices has several advantages on scalability and easiness of experiments with no need of an extreme vacuum as in the original cavity QED system. There, however, are a disadvantage that the system suffers strong environment noise. Environment noise is considered to strongly affect the fluorescence spectra of solid-state, and make its behavior qualitatively different from the atomic cavity QED. In Fig. 2.3, we show an example of a spectrum of an emitted photon from the cavity in applying a pump light whose frequency is tuned to excite a ground state of a quantum dot to an target excited state [50]. In usual experiments, the transition energy of a quantum dot is almost constant, whereas the cavity energy can be varied by changing the temperature, the intensity of pump light, and other experimental conditions. In the experiment shown in Fig. 2.3, quantity of condensate Xe on the surface is controlled to change the cavity energy. The peak changing its position depending on the Xe concentration corresponds to the cavity energy, and the other small invariant peaks correspond to the transition energies of a single quantum dot. One can clearly see a Rabi vacuum splitting when two peaks marge. Then, there is one mystery of this data; the cavity peak is not expected to appear if the detuning energy (the difference of the cavity and transition energy) is much larger than the linewidth of two peaks. The same feature has been observed in other experiments [39, 38, 40]. This feature is inherent in the cavity QED in solid state devices, and is not observed in the atomic cavity QED. Further experimental studies have characterized this peak more throughly [51, 52, 53, 54, 55, 56, 57] and now the appearance of fluorescence at the cavity frequency in the off-resonant condition is considered to be explained by dephasing effect due to the environment noise, which is unavoidable more or less in solid state devices.

In parallel to experimental studies, there have appeared several theoretical studies to account for the above experimental results on the photoluminescence spectra. Simple analyses based on the stochastic Schrödinger equation [58, 59] or the Master equation [60, 61, 62] has successfully explained appearance of the peak at the cavity frequency for the detuned case. These analyses implicitly assume white-noise type fluctuation as the environment noise, and are insufficient to explain details of experiments such as temperature dependences. More realistic model of the environment noise based on phonons [63, 64, 65, 66, 67] and charge fluctuation of background carriers [68] has also been studied. Whereas the understanding of photoluminescence spectra has thus been proceeding, dephasing effect on the indistinguishability of photons, which is crucial to the Hong-Ou-Mandel experiment on emitted photons from two single-photon generators, has not studied so far.

2.2 Single Electron Generation

2.2.1 Analogy between optics and electronics

In a long history of mesoscopic physics, which is a research area to study quantum nature of electrons in solids, analogy with optics has played an important role. For example, the term *Fabry-Perot interferometer*, which is realized in quantum wires with scatterers, was clearly imported from optics. In a level of one-particle interference experiments such as Young's interference experiments [69] (or the Aharonov-Bohm interference experiments [70]), there appears no difference between photons and electrons. On the other hand, important information of statistics of quantum particles is obtained from two-particle correlation. Therefore, the analogy with *quantum optics* has been utilized actively in study of *shot noise* in mesoscopic conductors [71, 72]. Two-particle correlation

Figure 2.4: Schematic of single-electron(hole) injection into an edge state. (a) Temporal change of a gate voltage applied to a quantum dot, (b) a schematic viewgraph of the experimental setup, and (c) energy diagram of electron(hole) injection. (Cited from Ref. [79]).

Figure 2.5: Experimental results of single electron generation. Temporal change of the gate voltage (the red lines), the averaged current (the black lines), and the fitted curve with exponential functions (the blue lines). (Cited from Ref. [79]).

has been measured in various types of experiments in mesoscopic systems such as shot noise reduction in point contacts [73], fermionic Hanbury Brown-Twiss experiments [74, 75], and two-particle Mach-Zender interferometer utilizing shot noise measurement [76, 77]. Now, there are a number of experimental supports on fermion statistics of electrons through quantum-optics-like experiments. We note that nonlocal quantum correlation breaking the Bell's inequality can be produced even from thermal source of electrons in, e.g., two-channel edge states [78].

Two-particle correlation measurement explained so far is for nonequilibrium steady state. Recently, there was one breakthrough in experiments on mesoscopic systems in *temporal* domain. In 2007, French experimental group has realized single electron sources by using a quantum dot and a time-controlled gate in order of sub-nanosecond [79]. Fig. 2.4 shows schematic of their experiment. They have applied the time-dependent gate voltage shown in Fig. 2.4 (a) to a quantum dot coupled to a chiral edge channel through a point contact (Fig. 2.4 (b)). Then, one electron and one hole are injected into a chiral edge channel in this period (Fig. 2.4 (c)) with appropriate tuning of the voltage-pulse amplitude. The average current induced in this temporal change of the gate voltage is shown in Fig. 2.5. At a rapid change of the gate-voltage (shown by the red lines), average additional currents are induced. The current shows exponential decay with finite decay rates, which are given as τ = 0.9ns, 3.6ns, and 10ns in the three graphs given in Fig. 2.5. The decay rates agree with theoretical values derived from the transmission probability D at a point contact, which has been estimated from the linear ac response. Moreover, the integral of the averaged current for a half of the period is shown to coincide with a charge e when the decay rate is sufficiently large.

Realization of dynamical control of electron(hole) injection opens up a novel type of experiments. The most important experiment in this category is the Hong-Ou-Mandel experiment explained in Chap. 1 (see Fig. 1.1), though it has not succeeded so far. With expectation of this novel type of quantum-optical experiments, several theoretical proposals such as two-particle collider shot noise [80] and nonlocal Aharonov-Bohm effect [81] have been presented. This experiment also provides a possibility of application to quantum information processing using moving electrons in edge channels.

After the experiment of Ref. [79], theoretical calculation based on noninteracting electron models [85, 87] and Master equations [86] has been performed to explain detailed feature of experiments of single-electron generation [88, 83, 84]. Although dephasing effect on injected single electrons has also been studied by several authors [88, 89], it is based on a phenomenological model using an additional bosonic port (see Sec. 2.1.1). In our knowledge, there is no theoretical trial so far to deal with Coulomb interaction effect, which is expected to be strong in single-electron injection process. We will study dephasing effect due to environment noise and Coulomb interaction in Chap. 4.

2.3 Fractional quantum Hall systems

Incompressive two-dimensional fluid in FQH effect has provided a number of interesting phenomena after its discovery [16]. This state emerges by drastic effect of Coulomb interaction between electrons in clean samples of two-dimensional electron gases under strong perpendicular mag-

Figure 2.6: Longitudinal and transverse resistivity of two-dimensional electron gases showing various hierarchical states of the FQH effect. (Cited from Ref. [94]).

Figure 2.7: Shot noise measurement for the $\nu = 1/3$ Laughlin state. (Cited from Ref. [19]).

netic field, and is described by Laughlin's wave functions [17] for a simple filling factor $\nu = 1/(1 + 2n)$. The hierarchical states of FQH has been considered in the picture of composite particles composed of electrons and some amount of flux, and have succeeded in explaining of experimental observation. We show an example of experimental observation on hierarchical structures of FQH states. We show an example of such hierarchical structures in FQH in Fig. 2.6.

One of the most remarkable properties in FQH states is existence of quasi-particle excitations with a fractional charge e^*. Direct measurement of fractional charge is possible in measurement of shot noise. We show one example of shot noise measurement for determination of fractional charge e^* at the $\nu = 1/3$ Laughlin state [19] in Fig. 2.7. Comparison with the theoretical prediction of shot noise power indicates that the fractional charge for the $\nu = 1/3$ Laughlin state seems to be not e but close to $e/3$.

The quasi-particle with fractional charges obeys fractional statistics [123], characterized by a statistical angle θ upon an adiabatic ex-

Figure 2.8: (a) Setup of the Aharonov Bohm for quasiparticles with fractional charges. (Cited from Ref. [22]). (b) Experimental setup for measurement of current cross-correlation to detect statistical angles. (Cited from Ref. [95]).

change process of two quasi-particles,

$$\Psi(r_1, r_2) = e^{i\theta}\Psi(r_2, r_1). \tag{2.3}$$

The issue to experimentally observe θ has also become an intriguing question. It has been proposed to use a kind of the Aharanov-Bohm (AB) effect in equilibrium [96, 97, 98, 99, 100] (Fig. 2.8 (a)), and has performed successfully in recent experiments [22, 101]. In order to further detect two-particle correlation between two fractional-charge excitations, a proposal to use cross-correlation of currents has been presented [95], though it has not been performed experimentally so far.

In Chap. 5, we study finite-temperature noise in FQH edge states. We propose another method to detect a statistical angle in experiments, by extending definition of shot noise into the finite-temperature regime.

Chapter 3

Single-Photon Generator

3.1 Introduction

As reviewed in the previous chapter, solid-state cavity QED systems composed of semiconductor quantum dots and cavities have recently been attracting much attention [6]. Strong coupling between a single dot and a cavity has been confirmed through a large vacuum Rabi splitting [39, 38, 40], and excellent performances have been reported in generating indistinguishable photons [90, 91] and entangled photon pairs [92], both of which are useful for quantum information processing [93].

In contrast with real atoms, semiconductor quantum dots are strongly influenced by environmental noise sources. The fluorescence spectra of solid-state and atomic cavity QED are qualitatively different. When a solid-state system is excited by a pump light of the dot frequency, a spectral peak appears at the cavity frequency in spite of the large detuning between them [39, 38, 40]. Further experimental studies have characterized this peak more throughly [51, 52, 53, 54, 55, 56, 57] and have revealed that the fluorescence at the cavity frequency is due to radiative decay of the dot. Subsequent theoretical studies accounted for pure dephasing of the dot through the stochastic Schrödinger equation [58, 59] or the Master equation [60, 61, 62] and successfully explained the peak at the cavity frequency. The influence of pure dephasing on radiative decay of the dot has also been understood in terms of the quantum Zeno and anti-Zeno effects [102, 60].

Therefore, when designing a single-photon source using solid-state cavity QED systems, it is crucial to quantitatively consider pure dephasing of the dot. The performance of such photon sources should be evaluated from two aspects. One is the collection efficiency; namely, the probability that the emitted photon is transferred to the intended spatial mode (i.e., the radiation pattern of the cavity). This has been discussed in several studies in terms of the ratio of radiative decay rates [58, 61, 62]. The other one is the indistinguishability of generated photons, which can be measured by two-photon interference experiments and is evaluated by the purity. Single photons with high purity are required for quantum information processing, particularly for constructing scalable quantum circuits.

In this chapter, we investigate the properties of a single photon emitted by a solid-state cavity QED system and quantitatively observe the effects of pure dephasing. We treat the five elements of the overall system (the dot, the cavity, radiation leaking from the cavity, non-cavity radiation modes, and the environment causing pure dephasing of the dot) as active quantum-mechanical degrees of freedom, and analytically derive the density matrix of the emitted photon in the real-space representation. This density matrix contains full information about the emitted photon, including its pulse profile, the frequency spectrum, and the purity. These quantities are observed as functions of the pure dephasing rate of the dot. We reveal the optimum condition for maximizing the purity of the emitted photon.

This chapter is organized as follows. In Sec.3.2, we introduce our model. In Sec.3.3, we analytically derive the state vector and the density matrix of the emitted photon in the real-space representation. This density matrix contains full information about the emitted photon, including its pulse profile, the frequency spectrum, and the purity. In Sec.3.4, we visualize analytical results for specific parameters. We reveal the optimum condition for maximizing the purity of the emitted photon. Finally in Sec.3.5 we summarize this chapter.

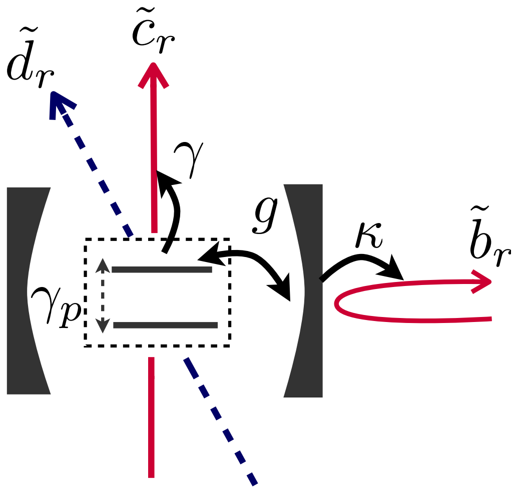

Figure 3.1: Schematic illustration of the solid-state cavity QED system considered. It consists of a quantum dot, a cavity, photon leakage from the cavity (b field), non-cavity radiation modes (c field), and a reservoir field, which causes pure dephasing of the dot (d field).

3.2 Model

We investigate radiative decay of an excited quantum dot placed inside a cavity, as illustrated in Fig. 3.1. This solid-state cavity QED system consists of the following five components: (i) a quantum dot, (ii) a cavity, (iii) a photon field leaking from the cavity (referred to as the b field hereafter), (iv) non-cavity radiation modes (c field), and (v) a reservoir field, which causes pure dephasing of the dot (d field) [104]. The annihilation operators corresponding to these components are respectively denoted by σ, a, b_k, c_k, and d_k, where k is a one-dimensional wavenumber. Note that σ is a Pauli operator, whereas the other operators are bosonic.

Putting $\hbar = c = 1$, the Hamiltonian of the overall system is given by

$$\mathcal{H} = \mathcal{H}_0 + \mathcal{H}_1 + \mathcal{H}_2 + \mathcal{H}_3, \tag{3.1}$$

$$\mathcal{H}_0 = \omega_d \sigma^\dagger \sigma + \omega_c a^\dagger a + g(\sigma^\dagger a + a^\dagger \sigma), \tag{3.2}$$

$$\mathcal{H}_1 = \int dk \left[k b_k^\dagger b_k + \sqrt{\kappa/(2\pi)}(a^\dagger b_k + b_k^\dagger a) \right], \tag{3.3}$$

$$\mathcal{H}_2 = \int dk \left[k c_k^\dagger c_k + \sqrt{\gamma/(2\pi)}(\sigma^\dagger c_k + c_k^\dagger \sigma) \right], \tag{3.4}$$

$$\mathcal{H}_3 = \int dk \left[k d_k^\dagger d_k + \sqrt{\gamma_p/\pi} \sigma^\dagger \sigma (d_k^\dagger + d_k) \right]. \tag{3.5}$$

The parameters are defined as follows (see Fig. 3.1). ω_d and ω_c respectively denote the resonance frequencies of the dot and the cavity, g represents the coupling between them, κ is the escape rate of cavity photons, γ is the radiative decay rate of the dot into non-cavity modes, and γ_p is the pure dephasing rate of the dot. $\mathcal{H}_0$ describes the Rabi oscillation between the dot and the cavity (Jaynes–Cummings Hamiltonian), $\mathcal{H}_1$ describes leakage of a cavity photon to its radiation pattern, $\mathcal{H}_2$ describes the radiative decay of the dot into unintended directions, and $\mathcal{H}_3$ describes pure dephasing of the dot. We can confirm that $\mathcal{N} \equiv \sigma^\dagger\sigma + a^\dagger a + \int dr \widetilde{b}_r^\dagger \widetilde{b}_r + \int dr \widetilde{c}_r^\dagger \widetilde{c}_r$ commutes with the Hamiltonian. Therefore, the number of excitations is conserved in the dot, cavity, b and c fields.

We assume that the dot is initially ($t = 0$) in the excited state while the other fields are in their vacuum states. Then, denoting the overall vacuum state by $|0\rangle$, the initial state vector is given by

$$|\psi_i\rangle = \sigma^\dagger |0\rangle. \tag{3.6}$$

The Hamiltonian of Eq. (3.1) and the initial state vector of Eq. (3.6) form the basis of our analysis.

For later convenience, we introduce the real-space representation of the b field (cavity leakage). It is defined by

$$\widetilde{b}_r = (2\pi)^{-1/2} \int dk e^{ikr} b_k. \tag{3.7}$$

The $r < 0$ ($r > 0$) region represents the incoming (outgoing) field. $\widetilde{c}_r$ and $\widetilde{d}_r$ can be formally defined in a similar manner. Our main concern lies in the properties of single photon emitted in the b field.

To model the pure dephasing of the dot, the d field interacts with the dot so as to conserve the dot excitation. Using Eqs. (3.2) and (3.5), the dot Hamiltonian can be rewritten as $[\omega_d + f(t)]\sigma^\dagger\sigma$, where $f(t) = \sqrt{2\gamma_p}[\widetilde{d}_0(t) + \widetilde{d}_0^\dagger(t)]$ is the fluctuation of the dot resonance frequency induced by the d field. Using Eqs. (3.6) and (3.10), we can confirm that $\langle f(t)f(t')\rangle_i = 2\gamma_p\delta(t-t')$, where $\langle\cdots\rangle_i = \langle\psi_i|\cdots|\psi_i\rangle$. Therefore, the present model assumes a white noise spectrum for fluctuation of the dot resonance.

3.3 Analysis

In this section, we present analytical results that are rigorously derivable from the model of Sec. 3.2. We solve the time evolution of the overall system and derive several formulae to characterize the emitted single photon (density matrix, pulse shape, spectrum, and purity). These analytical results are visualized in the next section for specific parameters.

3.3.1 Heisenberg equations

Here, we present the Heisenberg equations for the system (σ, a) and field (b_k, c_k, d_k) operators. Deriving the raw Heisenberg equations for the field operators from Eq. (3.1) and transforming them into real-space representations, we obtain the following relations that connect the incoming $(r < 0)$ and outgoing $(r > 0)$ fields:

$$\widetilde{b}_r(t) = \widetilde{b}_{r-t}(0) - i\sqrt{\kappa}\theta(r)\theta(t-r)a(t-r), \tag{3.8}$$

$$\widetilde{c}_r(t) = \widetilde{c}_{r-t}(0) - i\sqrt{\gamma}\theta(r)\theta(t-r)\sigma(t-r), \tag{3.9}$$

$$\widetilde{d}_r(t) = \widetilde{d}_{r-t}(0) - i\sqrt{2\gamma_p}\theta(r)\theta(t-r)\sigma^\dagger(t-r)\sigma(t-r), \tag{3.10}$$

where $\theta(x)$ is the Heaviside step function. From the raw Heisenberg equations for the system operators and the above input–output relations, the Heisenberg equations for system operators are given by

$$\frac{d}{dt}\sigma = -i\widetilde{\omega}_d\sigma - ig(1-2\sigma^\dagger\sigma)a \\ - i(1-2\sigma^\dagger\sigma)N_c(t) - i\left[N_d^\dagger(t)\sigma + \sigma^\dagger N_d(t)\right], \tag{3.11}$$

$$\frac{d}{dt}a = -i\widetilde{\omega}_c a - ig\sigma - iN_b(t), \tag{3.12}$$

where $\widetilde{\omega}_d = \omega_d - i(\gamma/2+\gamma_p)$ and $\widetilde{\omega}_c = \omega_c - i\kappa/2$ are respectively the complex frequencies of the dot and the cavity, and the noise operators are defined by $N_b(t) = \sqrt{\kappa}\widetilde{b}_{-t}(0)$, $N_c(t) = \sqrt{\gamma}\widetilde{c}_{-t}(0)$, and $N_d(t) = \sqrt{2\gamma_p}\widetilde{d}_{-t}(0)$. Note that the noise operators are the initial-time operators and consequently $N_j(t)|0\rangle = 0$ ($j = b, c, d$).

3.3.2 State vector

The state vector of the overall system at an arbitrary time t is determined by $|\psi(t)\rangle = e^{-i\mathcal{H}t}|\psi(0)\rangle$. Since the initial dot excitation is conserved in the dot, cavity, b, and c fields, the state vector can be written as

$$\left|\psi(t)\right\rangle = \left[\alpha_0(t)\sigma^\dagger + \beta_0(t)a^\dagger + \int dr\gamma_0(r,t)\widetilde{b}_r^\dagger + \int dr\delta_0(r,t)\widetilde{c}_r^\dagger\right]|0\rangle \\ + \sum_{m=1}^{\infty}\int d^m\boldsymbol{x}\left[\alpha_m(\boldsymbol{x},t)\sigma^\dagger + \beta_m(\boldsymbol{x},t)a^\dagger + \right. \\ \left.\int dr\gamma_m(r,\boldsymbol{x},t)\widetilde{b}_r^\dagger + \int dr\delta_m(r,\boldsymbol{x},t)\widetilde{c}_r^\dagger\right]\widetilde{d}_{x_1}^\dagger\cdots\widetilde{d}_{x_m}^\dagger|0\rangle, \tag{3.13}$$

where m denotes the number of excitations in the d field and $\int d^m\boldsymbol{x}$ denotes a multi-dimensional integral with respect to $\boldsymbol{x} = (x_1, x_2, \cdots, x_m)$. We can set $x_1 \le \cdots \le x_m$ without loss of generality. As we show later, these coefficients are nonzero only when $0 \le r \le x_1 \le \cdots \le x_m \le t$.

First, we discuss α_0 and β_0. From Eq. (3.13), we can confirm that $\alpha_0(t) = \langle\sigma(t)\sigma^\dagger(0)\rangle$ and $\beta_0(t) = \langle c(t)\sigma^\dagger(0)\rangle$, where $\langle\cdots\rangle = \langle 0|\cdots|0\rangle$. From Eqs. (3.11) and (3.12), their equations of motion are given by

$$\frac{d}{dt}\begin{pmatrix}\alpha_0(t)\\ \beta_0(t)\end{pmatrix} = \begin{pmatrix}-i\widetilde{\omega}_d & -ig\\ -ig & -i\widetilde{\omega}_c\end{pmatrix}\begin{pmatrix}\alpha_0(t)\\ \beta_0(t)\end{pmatrix}, \tag{3.14}$$

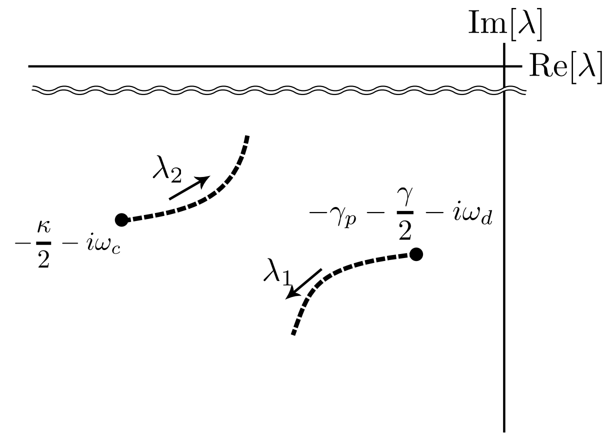

Figure 3.2: λ_1 and λ_2 in the complex plane. $\lambda_1 = -i\widetilde{\omega}_d$ and $\lambda_2 = -i\widetilde{\omega}_c$ when $g = 0$. Dotted lines show their traces as g increases.

with the initial conditions $\alpha_0(0) = 1$ and $\beta_0(0) = 0$. The solutions are given by

$$\alpha_0(t) = A_1 e^{\lambda_1 t} + A_2 e^{\lambda_2 t}, \tag{3.15}$$

$$\beta_0(t) = B_1 e^{\lambda_1 t} + B_2 e^{\lambda_2 t}, \tag{3.16}$$

where λ_1 and λ_2 are the two eigenvalues of the 2×2 matrix in Eq. (3.14) (see Fig. 3.2), $A_1 = (\lambda_1 + i\widetilde{\omega}_c)/(\lambda_1 - \lambda_2)$, $A_2 = (\lambda_2 + i\widetilde{\omega}_c)/(\lambda_2 - \lambda_1)$, and $B_1 = -B_2 = -ig/(\lambda_1 - \lambda_2)$. The real parts of λ_1 and λ_2 are always negative and consequently α_0 and β_0 vanish as $t \to \infty$. Equation (3.13) also implies that $\gamma_0(r,t) = \langle \widetilde{b}_r(t)\sigma^\dagger(0)\rangle$ and $\delta_0(r,t) = \langle \widetilde{c}_r(t)\sigma^\dagger(0)\rangle$. From Eqs. (3.8) and (3.9), we have

$$\gamma_0(r,t) = -i\sqrt{\kappa}\beta_0(t-r), \tag{3.17}$$

$$\delta_0(r,t) = -i\sqrt{\gamma}\alpha_0(t-r). \tag{3.18}$$

Rigorously, $\theta(r)\theta(t-r)$ should appear on the right-hand sides of these equations. However, below, we implicitly assume $0 \le r \le x_1 \le \cdots \le x_m \le t$ and omit the Heaviside functions.

Next, we proceed to investigate higher-order quantities. We consider α_1 and β_1 as examples. Applying the same reasoning as that for γ_0 and δ_0, we have $\alpha_1(x,t) = -i\sqrt{2\gamma_p}\langle\sigma(t)\sigma^\dagger(t-x)\sigma(t-x)\sigma^\dagger(0)\rangle$

and $\beta_1(x,t) = -i\sqrt{2\gamma_p}\langle a(t)\sigma^\dagger(t-x)\sigma(t-x)\sigma^\dagger(0)\rangle$. Thus, we need to evaluate the two-time correlation functions, $\langle\sigma(t_2)\sigma^\dagger(t_1)\sigma(t_1)\sigma^\dagger(0)\rangle$ and $\langle a(t_2)\sigma^\dagger(t_1)\sigma(t_1)\sigma^\dagger(0)\rangle$ with $t_2 > t_1 > 0$. Their equations of motion with respect to t_2 have the same form as Eq. (3.14) and their initial values ($t_2 \to t_1$) are $\alpha_0(t_1)$ and 0, respectively. This implies that the two-time correlation functions can be factorized as $\langle\sigma(t_2)\sigma^\dagger(t_1)\sigma(t_1)\sigma^\dagger(0)\rangle = \alpha_0(t_2-t_1)\alpha_0(t_1)$ and $\langle a(t_2)\sigma^\dagger(t_1)\sigma(t_1)\sigma^\dagger(0)\rangle = \beta_0(t_2-t_1)\alpha_0(t_1)$. Thus, we have

$$\alpha_1(x,t) = -i\sqrt{2\gamma_p}\alpha_0(t-x)\alpha_0(x), \tag{3.19}$$

$$\beta_1(x,t) = -i\sqrt{2\gamma_p}\alpha_0(t-x)\beta_0(x). \tag{3.20}$$

Repeating the same arguments, all coefficients can be written as products of α_0 and β_0, as follows:

$$\alpha_m(\boldsymbol{x},t) = \left(-i\sqrt{2\gamma_p}\right)^m \alpha_0(t-x_m)\alpha_0(x_m-x_{m-1})\cdots\alpha_0(x_2-x_1)\alpha_0(x_1), \tag{3.21}$$

$$\beta_m(\boldsymbol{x},t) = \left(-i\sqrt{2\gamma_p}\right)^m \alpha_0(t-x_m)\alpha_0(x_m-x_{m-1})\cdots\alpha_0(x_2-x_1)\beta_0(x_1), \tag{3.22}$$

$$\gamma_m(r,\boldsymbol{x},t) = \left(-i\sqrt{\kappa}\right)\left(-i\sqrt{2\gamma_p}\right)^m \alpha_0(t-x_m)\alpha_0(x_m-x_{m-1})\cdots\alpha_0(x_2-x_1)\beta_0(x_1-r), \tag{3.23}$$

$$\delta_m(r,\boldsymbol{x},t) = \left(-i\sqrt{\gamma}\right)\left(-i\sqrt{2\gamma_p}\right)^m \alpha_0(t-x_m)\alpha_0(x_m-x_{m-1})\cdots\alpha_0(x_2-x_1)\alpha_0(x_1-r). \tag{3.24}$$

3.3.3 Decay of dot excitation

The state vector of Eq. (3.13) fully describes the dynamics of the overall system, including both its transient and asymptotic behaviors. In this section, as an example of a transient phenomenon, we analyze the decay of the dot excitation. The survival probability of the dot excitation is defined as

$$P(t) = \langle\psi(t)|\sigma^\dagger\sigma|\psi(t)\rangle. \tag{3.25}$$

From Eqs. (3.13) and (3.21), we have

$$P(t) = |\alpha_0(t)|^2 + 2\gamma_p \int dx |\alpha_0(t-x)|^2 |\alpha_0(x)|^2 + \cdots . \tag{3.26}$$

We here introduce the Laplace transform of $|\alpha_0|^2$, which is defined by $\mathcal{L}_{|\alpha_0|^2}(z) = \int_0^\infty dt e^{-zt} |\alpha_0(t)|^2$. It is given by

$$\mathcal{L}_{|\alpha_0|^2}(z) = \sum_{m,n=1,2} \frac{A_m A_n^*}{z - \lambda_m - \lambda_n^*}, \tag{3.27}$$

where $\lambda_{1,2}$ and $A_{1,2}$ are defined in Sec. 3.3.2. The Laplace transform of $P(t)$ is then given by

$$\mathcal{L}_P(z) = \frac{\mathcal{L}_{|\alpha_0|^2}(z)}{1 - 2\gamma_p \mathcal{L}_{|\alpha_0|^2}(z)}. \tag{3.28}$$

$P(t)$ is obtained by analyzing the poles of this function in the z-plane. We denote the four roots of the equation $1 - 2\gamma_p \mathcal{L}_{|\alpha_0|^2}(z) = 0$ by μ_j ($j = 1, \cdots, 4$) (see Fig. 3.3). $P(t)$ is then given by

$$P(t) = \sum_{j=1}^{4} E_j e^{\mu_j t}, \tag{3.29}$$

$$E_j = \frac{\prod_{m',n'=1,2} (\mu_j - \lambda_{m'} - \lambda_{n'}^*)}{\prod_{i(\neq j)} (\mu_j - \mu_i)} \sum_{m,n=1,2} \frac{A_m A_n^*}{\mu_j - \lambda_m - \lambda_n^*}. \tag{3.30}$$

Note that the real parts of μ_j are always negative and that the survival probability $P(t)$ vanishes in the $t \to \infty$ limit, as expected.

3.3.4 Density matrix of emitted photon

In the $t \to \infty$ limit, the initial dot excitation is completely transformed into a photon propagating in the intended mode (b field) or in unintended directions (c field). In the following subsections, we analyze the photon emitted in the b-field. It is fully characterized by its density matrix $\hat{\rho}(t)$. In the real space representation, the matrix element $\rho(r, r', t)$ is given by

$$\rho(r, r', t) = \langle \psi(t) | \widetilde{b}_{r'}^\dagger \widetilde{b}_r | \psi(t) \rangle. \tag{3.31}$$

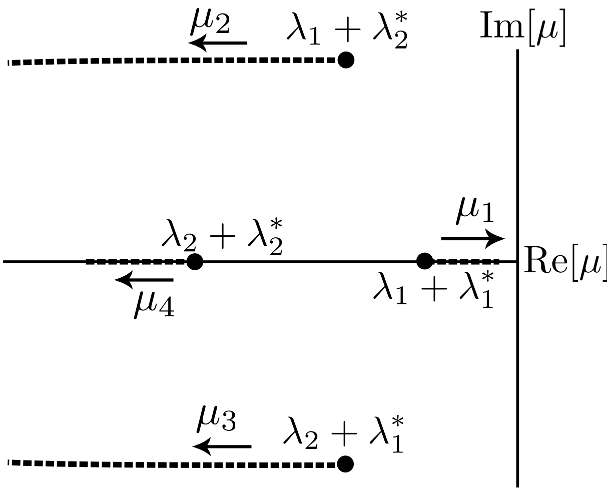

Figure 3.3: μ_j $(j = 1, \cdots, 4)$ in the complex plane. When γ_p is absent, $\mu_1 = \lambda_1 + \lambda_1^*$, $\mu_2 = \lambda_1 + \lambda_2^*$, $\mu_3 = \lambda_2 + \lambda_1^*$, and $\mu_4 = \lambda_2 + \lambda_2^*$. Dotted lines indicate their traces as γ_p increases. Real parts of μ_j are always negative for any γ_p.

We make the following three comments regarding this quantity: (i) $\hat{\rho}(t)$ is Hermitian, namely $\rho(r', r, t) = \rho^*(r, r', t)$. Therefore, we need consider only the $r < r'$ region in this subsection. (ii) As we will see later, $\rho(r, r', t) = \rho(r - t, r' - t)$ in the $t \to \infty$ limit. This reflects translational motion of the emitted photon. (iii) $\mathrm{Tr}\hat{\rho}(t) = \int dr \rho(r, r, t)$ represents the probability of finding the emitted photon in the b field. This is unity when $\gamma = 0$.

Using Eqs. (3.13) and (3.23), the matrix element can be rewritten as

$$\rho(r, r', t) = \kappa\beta_0(t - r)\beta_0^*(t - r') + 2\gamma_p\kappa \int dx \beta_0(x - r)\beta_0^*(x - r')|\alpha_0(t - x)|^2 + \cdots . \tag{3.32}$$

We here introduce the Laplace transform of $\beta_0\beta_0^*$, which is defined by $\mathcal{L}_{\beta_0\beta_0^*}(r, r', z) = \int_0^\infty dt e^{-zt}\beta_0(t - r)\beta_0^*(t - r')$. It is given by

$$\mathcal{L}_{\beta_0\beta_0^*}(r, r', z) = \sum_{m,n=1,2} \frac{B_m B_n^*}{z - \lambda_m - \lambda_n^*} e^{\lambda_m(r' - r) - r'z}, \tag{3.33}$$

where $\lambda_{1,2}$ and $B_{1,2}$ are defined in Sec. 3.3.2. The Laplace transform of

$\rho(r, r', t)$ is then given by

$$\mathcal{L}_\rho(r, r', z) = \frac{\kappa \mathcal{L}_{\beta_0\beta_0^*}(r, r', z)}{1 - 2\gamma_p \mathcal{L}_{|\alpha_0|^2}(z)}. \tag{3.34}$$

By analyzing the poles of this function in the z-plane, $\rho(r, r', t)$ is obtained as follows:

$$\rho(r, r', t) = \sum_{j=1}^{4} \sum_{m=1}^{2} \rho_{jm} e^{\lambda_m (r'-r) - \mu_j (t-r')}, \tag{3.35}$$

$$\rho_{jm} = \frac{\prod_{m',n'=1,2}(\mu_j - \lambda_{m'} - \lambda_{n'}^*)}{\prod_{i(\neq j)}(\mu_j - \mu_i)} \sum_{n=1}^{2} \frac{B_m B_n^*}{\mu_j - \lambda_m - \lambda_n^*}, \tag{3.36}$$

where $0 < r < r' < t$ and μ_j $(j = 1, \cdots, 4)$ are defined in Sec. 3.3.3. We can check that this quantity depends on only two variables, $r - t$ and $r' - t$.

3.3.5 Pulse shape

The pulse shape of the emitted photon is characterized by the intensity distribution

$$f(r, t) = \langle \psi(t) | \widetilde{b}_r^\dagger \widetilde{b}_r | \psi(t) \rangle = \rho(r, r, t), \tag{3.37}$$

which is the diagonal element of the density matrix. This quantity is real and positive in $0 < r < t$. By setting $r' = r$ in Eq. (3.35), we have

$$f(r, t) = \sum_{j=1}^{4} f_j e^{-\mu_j (t-r)}, \tag{3.38}$$

$$f_j = \frac{\prod_{m',n'=1,2}(\mu_j - \lambda_{m'} - \lambda_{n'}^*)}{\prod_{i \neq j}(\mu_j - \mu_i)} \sum_{m,n=1}^{2} \frac{B_m B_n^*}{\mu_j - \lambda_m - \lambda_n^*}. \tag{3.39}$$

3.3.6 Frequency Spectrum

The frequency spectrum of the emitted photon is defined by

$$S(k, t) = \langle \psi(t) | b_k^\dagger b_k | \psi(t) \rangle. \tag{3.40}$$

Apparently, $S(k,t)$ becomes independent of t in the $t \to \infty$ limit, and we are interested in $S(k) = \lim_{t\to\infty} S(k,t)$. By definition, $S(k,t)$ is the Fourier transform of the density matrix element:

$$S(k,t) = \frac{1}{2\pi} \iint drdr' e^{ik(r'-r)} \rho(r,r',t). \tag{3.41}$$

We consider the Laplace transform of $S(k,t)$ defined by $\mathcal{L}_S(k,z) = \int_0^\infty dte^{-zt} S(k,t)$. Using Eqs. (3.34) and (3.41), it is given by

$$\mathcal{L}_S(k,z) = \frac{\kappa}{2\pi} \frac{\mathcal{L}'_{\beta_0\beta_0^*}(k,z)}{1 - 2\gamma_p \mathcal{L}_{|\alpha_0|^2}(z)}, \tag{3.42}$$

where

$$\begin{aligned} \mathcal{L}'_{\beta_0\beta_0^*}(k,z) &= \int_0^\infty dt \iint drdr' e^{ik(r'-r)-zt} \beta_0^*(t-r')\beta_0^*(t-r) \\ &= \int_0^\infty dte^{-zt} \left| \sum_{m=1}^{2} \frac{B_m}{\lambda_m + ik} (e^{-ikt} - e^{\lambda_m t}) \right|^2. \end{aligned} \tag{3.43}$$

Note that $\mathcal{L}'_{\beta_0\beta_0^*}$ has a pole at $z = 0$. Since our interest lies in the $t \to \infty$ limit of $S(k,t)$, we need to investigate the pole of $\mathcal{L}_S(k,z)$ at $z = 0$ only. Therefore, $S(k) = (\kappa/2\pi)[1 - 2\gamma_p \mathcal{L}_{|\alpha_0|^2}(0)]^{-1} \operatorname{Res}_{z=0}[\mathcal{L}'_{\beta_0\beta_0^*}(k,z)]$. After some calculations, we obtain

$$S(k) = \frac{\mathcal{N}}{|(k-\widetilde{\omega}_d)(k-\widetilde{\omega}_c) - g^2|^2}, \tag{3.44}$$

where $\mathcal{N} = (\kappa g^2/2\pi)[1 - 2\gamma_p \mathcal{L}_{|\alpha_0|^2}(0)]^{-1}$ is a factor that is independent of k. This spectral shape was predicted by Glauber [103], and it was confirmed in recent theoretical studies based on the quantum Langevin equations [58, 59] and the Master equations [60, 61, 62].

3.3.7 Purity

Quantum information processing requires high indistinguishability between single photons. A popular measure of indistinguishability of photons is the coincidence probability P_{co} in two-photon interference experiments (see Fig. 3.4). When two indistinguishable photons are simultaneously input to a beamsplitter, they always appear at the same

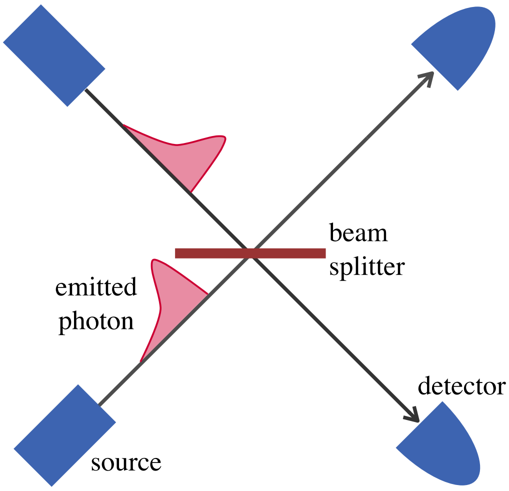

Figure 3.4: Schematic illustration of two-photon interference experiment. The coincidence probability vanishes when the two input photons are completely indistinguishable.

output port (Hong–Ou–Mandel interference), namely, $P_{co} = 0$. However, pure dephasing generates entanglement between an emitted photon and the environment of its source, and it makes two-photon interference imperfect ($P_{co} > 0$). The coincidence probability is related to the purity $\mathcal{P}$ of a photon by $P_{co} = (1 - \mathcal{P})/2$ (see Appendix 3.A for the derivation).

The purity is defined in terms of the density matrix $\hat{\rho}(t)$ by

$$\mathcal{P} \equiv \frac{\mathrm{Tr}[\hat{\rho}^2(t)]}{\mathrm{Tr}[\hat{\rho}(t)]^2}. \tag{3.45}$$

As expected, this quantity becomes independent of t when t is sufficiently large. Using the real-space matrix element, the purity can be rewritten as

$$\mathcal{P} = \frac{\int drdr' \rho(r,r',t)\rho(r',r,t)}{\left[\int dr \rho(r,r,t)\right]^2} = \frac{\int drdr' |\rho(r,r',t)|^2}{\left[\int dr \rho(r,r,t)\right]^2}. \tag{3.46}$$

Using Eq. (3.36), we have

$$\mathcal{P} = \frac{\mathcal{P}_n}{\mathcal{P}_d}, \tag{3.47}$$

$$\mathcal{P}_n = \sum_{j,j'=1}^{4} \sum_{m,m'=1}^{2} \frac{2\rho_{jm}\rho^*_{j'm'}}{(\mu_j + \mu^*_{j'})(\lambda_m + \lambda^*_{m'})}, \tag{3.48}$$

$$\mathcal{P}_d = \sum_{j=1}^{4} \sum_{m=1}^{2} \frac{\rho_{jm}}{-\mu_j}. \tag{3.49}$$

$\mathcal{P}_d$ is an efficiency of two photons to go into the intended modes and $\mathcal{P}_d = 1$ if $\gamma = 0$.

3.4 Numerical results

The analytical results derived in the previous section are rigorous and applicable to any set of parameters, $(\omega_d - \omega_c, g, \kappa, \gamma, \gamma_p)$. In this section, we visualize these results by employing specific parameters. Throughout this section, we assume for simplicity that radiative decay to unintended modes does not occur ($\gamma = 0$).

3.4.1 Zeno and Anti-Zeno effects

First, we observe the effects of pure dephasing on decay of the dot excitation. We focus on the weak-coupling regime ($\kappa = 6g$) in this subsection, where the dot decays monotonically without revival and obeys the exponential decay law to a high accuracy. The decay rate of the dot is well defined in this case and is given by $\Gamma = \lim_{t\to\infty}[-\log P(t)/t]$. This reduces to $\min_j |\mathrm{Re}\,\mu_j|$, where μ_j is defined in Sec. 3.3.3.

Figure 3.5 shows the temporal behavior of the survival probability $P(t)$. In Fig. 3.5(a), where the dot is in resonance with the cavity ($\omega_d = \omega_c$), the decay becomes slower as pure dephasing increases. In contrast, in Fig. 3.5(b), where the dot is detuned from the cavity ($\omega_d - \omega_c = 600$ μeV), the decay becomes faster under small pure dephasing ($\gamma_p = 200$ μeV), whereas the decay becomes slower under larger pure dephasing

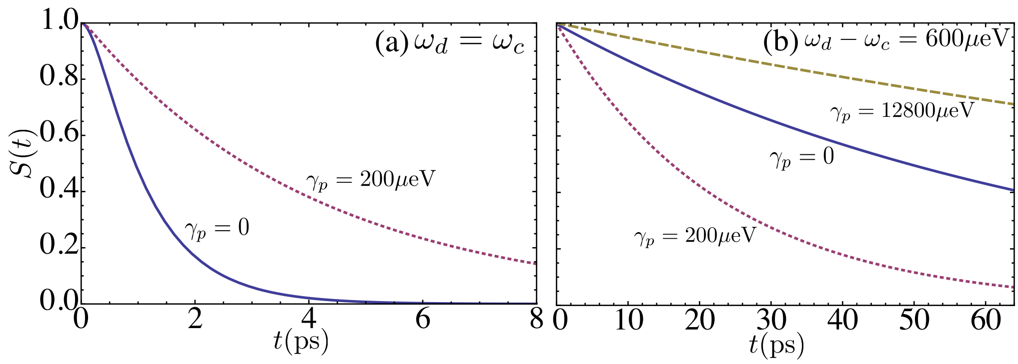

Figure 3.5: Survival probability $S(t)$ for (a) resonant ($\omega_d = \omega_c$) and (b) detuned ($\omega_d - \omega_c = 600$ μeV) cases. $g = 25$ μeV and $\kappa = 150$ μeV. The values of γ_p are indicated in the figures.

($\gamma_p = 12800$ μeV). Such suppression and enhancement of decay can be interpreted as the quantum Zeno and anti-Zeno effects, since pure dephasing plays the same role as repeated measurements in destroying quantum coherence [102, 60]. Previous analyses predict that the anti-Zeno effect can be observed only when the dot–cavity detuning is large and pure dephasing is small [102]. This agrees with the present numerical results.

Figure 3.6 shows the dependence of the radiative decay rate Γ on the pure-dephasing rate γ_p. To clearly observe the Zeno and anti-Zeno effects, $\Gamma(\gamma_p)$ is normalized by the *free* decay rate of $\Gamma(0)$: $\Gamma(\gamma_p)/\Gamma(0) < 1$ indicates the Zeno effect, whereas $\Gamma(\gamma_p)/\Gamma(0) > 1$ exhibits the anti-Zeno effect. Non-monotonous behavior of $\Gamma(\gamma_p)$ is clearly observed for large detuning.

3.4.2 Pulse shape and spectrum

In this subsection, we examine the pulse shape and the frequency spectrum of the emitted photon using the same parameters as those used in the previous subsection. First, we observe the results for the resonant ($\omega_d = \omega_c$) case. The pulse shapes $f(r,t)$ of the emitted photon are shown in Fig. 3.7(a) for three pure dephasing rates γ_p. Each pulse shape is nor-

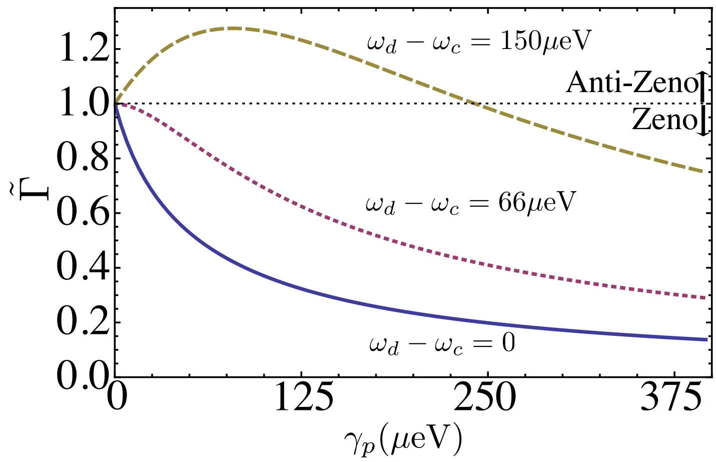

Figure 3.6: Dependence of the radiative decay rate $\tilde{\Gamma}$ on the pure-dephasing rate γ_p. The radiative decay rate is normalized by the *free* decay rate (i.e., the rate for $\gamma_p = 0$). $g = 25$ μeV and $\kappa = 150$ μeV. $\omega_d - \omega_c = 0$ (solid), 66 μeV (dotted) and 150 μeV (dashed).

malized $[\int_{-\infty}^{t} dr f(r,t) = 1]$ since $\gamma = 0$ is assumed here and a single photon is necessarily generated in the b field. The pulse becomes longer as pure dephasing increases. This is consistent with the quantum Zeno effect discussed in the previous subsection: In the resonant case, the decay of the dot becomes monotonously slower with increasing pure dephasing. Figure 3.7(b) shows the spectra $S(k)$ of the photon for the same parameters as Fig. 3.7(a). These spectra have a single peak at $k = \omega_d (= \omega_c)$ and are normalized $[\int_{-\infty}^{\infty} dk S(k) = 1]$. The spectrum broadens with increasing pure dephasing. This is confirmed by Fig. 3.7(c) in which the spectral width (defined as $\Delta = [\int dk (k - \omega_d)^2 S(k)]^{1/2}$) is plotted as a function of the pure dephasing rate. Thus, the pulse broadens in both real and frequency spaces with increasing γ_p and it is thus not Fourier-limited. This implies the mixedness of the emitted photon when $\gamma_p \neq 0$. The purity of the photon is discussed later in Sec. 3.4.3.

Next, we observe the results for the detuned case. Figure 3.8 (a) shows the pulse shapes of the photon. The pulse shape is approximately exponential except for the oscillatory behavior at the very initial

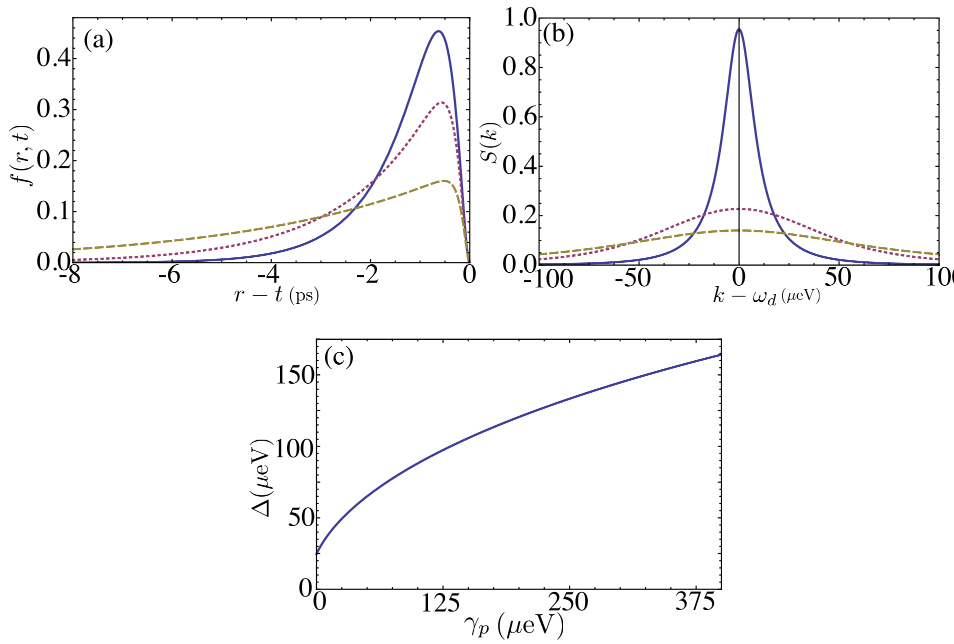

Figure 3.7: (a) Pulse shape $f(r,t)$ and (b) spectrum $S(k)$ of emitted photon. $g = 25\ \mu$eV, $\kappa = 150\ \mu$eV and $\omega_d - \omega_c = 0$. $\gamma_p = 0$ (solid), 50 μeV (dotted), and 200 μeV (dashed). (c) Spectral width as a function of γ_p.

stage. The pulse length is inversely proportional to the decay rate of the dot. Figure 3.8(b) shows the photon spectra for the same parameters as Fig. 3.8(a). A notable difference from the resonant cases is that the spectra are doubly peaked with peaks at both the dot frequency ω_d and the cavity frequency ω_c. The widths of these peaks are determined by $|\mathrm{Im}\widetilde{\omega}_d| = \gamma/2+\gamma_p$ and $|\mathrm{Im}\widetilde{\omega}_c| = \kappa/2$. Therefore, the width of the peak at ω_d is sensitive to pure dephasing. When pure dephasing is weak ($\gamma_p \ll \kappa/2$) as in atomic cavity QED systems, the dominant peak of $S(k)$ appears at ω_d. In contrast, when pure dephasing is strong ($\gamma_p \gg \kappa/2$) as in solid-state systems, the dominant peak of $S(k)$ appears at ω_c. This partly explains the detuned peaks observed in the resonance fluorescence spectrum in solid-state cavity QED systems.

The mean energy of the emitted photon is evaluated by $E_p = \int dk\, kS(k)$. Due to energy conservation, the mean photon energy is expected to al-

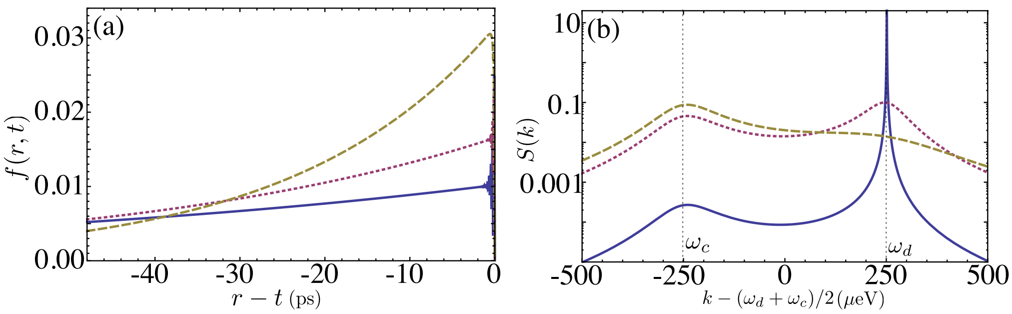

Figure 3.8: (a) Pulse shape $f(r,t)$ and (b) spectrum $S(k)$ of emitted photon. $g = 25$ μeV, $\kappa = 150$ μeV and $\omega_d - \omega_c = 600$ μeV. $\gamma_p = 0$ (solid), 50 μeV (dotted), and 200 μeV (dashed).

ways be identical to the dot frequency (i.e., $E_p = \omega_d$). However, Fig. 3.8(b) clearly shows that the mean photon energy is sensitive to pure dephasing and may deviate from the dot frequency when pure dephasing is present. This discrepancy can be resolved by considering the energy released to the environment during decay, which is given by $E_e = \int dk\, k \langle d_k^\dagger d_k \rangle$. It can be shown that (see Appendix 3.B for derivation)

$$E_p = \frac{\kappa}{\kappa + 2\gamma_p}\omega_d + \frac{2\gamma_p}{\kappa + 2\gamma_p}\omega_c, \tag{3.50}$$

$$E_e = \frac{2\gamma_p}{\kappa + 2\gamma_p}(\omega_d - \omega_c). \tag{3.51}$$

Thus, energy conservation is satisfied when the environmental energy is included ($E_p + E_e = \omega_d$). An important insight here is that while pure dephasing coupling never induces a transition in the dot, this coupling enables energy exchange between the dot and the environment. When the cavity frequency exceeds the dot frequency, Eq. (3.51) indicates that the dot may absorb environmental energy during decay [104].

3.4.3 Purity

The pulse shape and spectrum presented in Figs. 3.7(a) and (b), respectively, indicate that the emitted photon is not Fourier limited when pure dephasing is present and it is thus in a mixed state. Here, we observe

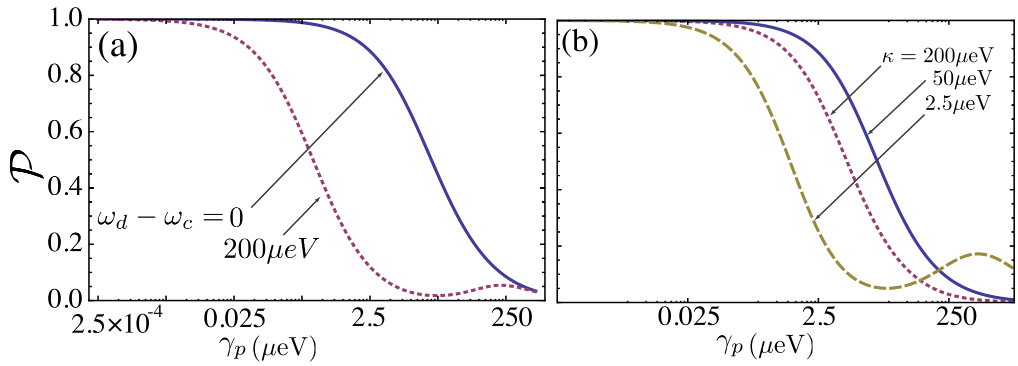

Figure 3.9: Dependences of the purity on γ_p. In (a), g and κ are fixed (g = 25 μeV, κ = 50 μeV) and the detuning is varied: $\omega_d - \omega_c = 0$ (solid) and 200 μeV (dotted). In (b), g and $\omega_d - \omega_c$ are fixed (g = 25 μeV, $\omega_d - \omega_c = 0$) and κ is varied: κ = 50 μeV (solid), 200 μeV (dotted) and 2.5 μeV (dashed).

how the purity of the emitted photon depends on the system parameters. The purity is approximately determined by the product of τ (dot excitation lifetime before it leaves the cavity) and γ_p (pure dephasing rate): $\mathcal{P} \simeq 1$ when $\gamma_p\tau \ll 1$, whereas $\mathcal{P} \simeq 0$ when $\gamma_p\tau \gg 1$. In Fig. 3.9(a), the purity is plotted as a function of γ_p by fixing the escape rate of the cavity photon (κ = 50 μeV) and varying the detuning $\omega_d - \omega_c$. As expected, the purity is unity in the $\gamma_p \to 0$ limit and decreases with increasing γ_p. Detuning between the dot and cavity reduces the purity of the emitted photon because the excitation lifetime τ increases with increasing detuning. In Fig. 3.9(b), the purity is plotted as a function of γ_p by assuming there is no detuning ($\omega_d = \omega_c$) and varying κ. The purity is maximized when κ = 50 μeV, where is comparable to g. This can be understood as follows: When $\kappa \ll g$, the excitation lifetime τ increases and the purity is degraded due to the long lasting Rabi oscillation between the dot and the cavity. In contrast, when $\kappa \gg g$, τ increases due to overdamping. The optimal value of κ is more clearly seen in Fig. 3.10, where the purity is plotted as a function of κ for several values of γ_p. The purity is maximized when κ is comparable to g, regardless of γ_p.

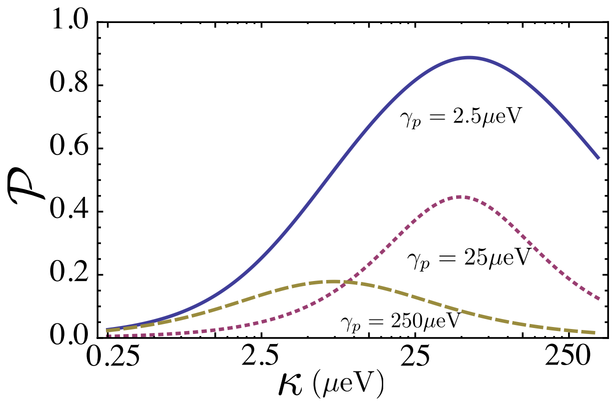

Figure 3.10: Dependences of the purity on κ. g and $\omega_d - \omega_c$ are fixed ($g = 25$ μeV, $\omega_d - \omega_c = 0$). $\gamma_p = 2.5$ μeV (solid), 25 μeV (dotted), and 250 μeV (dashed).

3.4.4 Time filtering

In order to increase the purity of emitted photons, one effective way is only to use photons emitted into an output channel in an early stage, because such a photon has no time to be affected by dephasing due to the environment. The purity of photons filtered in the temporal regime $0 \le t \le T$ is written as

$$\mathcal{P}(T) = \frac{\mathcal{P}_n(T)}{\mathcal{P}_d(T)}, \tag{3.52}$$

$$\mathcal{P}_n(T) = \frac{2\rho_{jm}\rho^*_{j'm'}}{(\lambda_m + \lambda^*_{m'})}\left[\frac{1 - e^{(\mu_j+\mu^*_{j'})t}}{\mu_j + \mu^*_{j'}} + \frac{e^{(\lambda_m+\lambda^*_{m'})t} - e^{(\mu_j+\mu^*_{j'})t}}{\lambda_m + \lambda^*_{m'} - \mu_j - \mu^*_{j'}}\right], \tag{3.53}$$

$$\mathcal{P}_d(T) = \left(\sum_{j=1}^{4}\sum_{m=1}^{2}\frac{\rho_{jm}}{-\mu_j}(1 - e^{\mu_j t})\right)^2. \tag{3.54}$$

The denominator $\mathcal{P}_d(T)$ is a square of a probability that a photon is emitted during $0 \le t \le T$, and equals to a probability that *both* of two photon sources produce one photon. We call $\mathcal{P}_d(T)$ a efficiency of time filtering. Although the numerator $\mathcal{P}_n(T)$ is always smaller than $\mathcal{P}_n(\infty)$, the total purity $\mathcal{P}(T)$ is improved from $\mathcal{P}_d(\infty)$ as the denominator $\mathcal{P}_d(T)$ becomes smaller than 1.

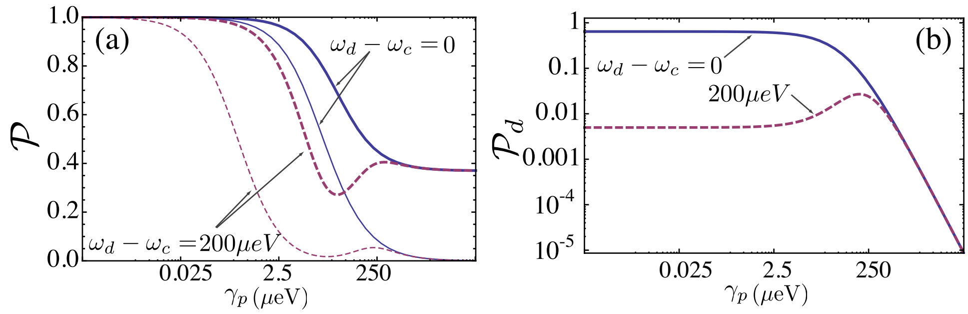

Figure 3.11: (a) Purities $\mathcal{P}(T)$ and (b) efficiencies $\mathcal{P}_d(T)$ as a function of γ_p. The detuning is taken as $\omega_d - \omega_c = 0$ (solid) and 200 μeV (dotted) by fixing g and κ ($g = 25$ μeV, $\kappa = 50$ μeV). In the figure (a), thin and thick lines show the purity without filtering and with time filtering ($T = 2/g$), respectively.

Fig. 3.11(a) shows the improved purity when the filtering time is taken as $T = 2/g$, and other parameters are taken as the same as Fig. 3.9 (a). Both in the on-resonant and off-resonant case, the purity is improved by time filtering and converged to a finite value in the limit of $\gamma_p \to \infty$. Fig. 3.11(b) shows the efficiency $\mathcal{P}_d(T)$. The efficiency decreases exponentially in the limit of $\gamma_p \to \infty$. This can be understood by increase of the decay time due to the Zeno effect.

In actual experiments, time filtering with too small T is not realistic, because the efficiency $\mathcal{P}_d(T)$ gets small down to an unacceptable level. Fig. 3.12 shows the improved purity with fixed efficiency ($\mathcal{P}_d(T) = 1/2$) as a function of γ_p. Maximum magnification of the purity is expected naively to be an inverse of the efficiency. This maximum is achieved when γ_p is large, however, in that case T is also large. Too large filtering time T is also unrealistic, because in real experiment there is a spontaneous emission into a vacuum with a finite rate γ, neglected in the present calculation. Probably, the optimum value of T is of order of $1/g$. If we need photons whose purity $\mathcal{P} > 0.6$, the pure dephasing rate must be less than $0.03g$ without filtering, however, with filtering, pure dephasing rate can be large within $< 0.08g$.

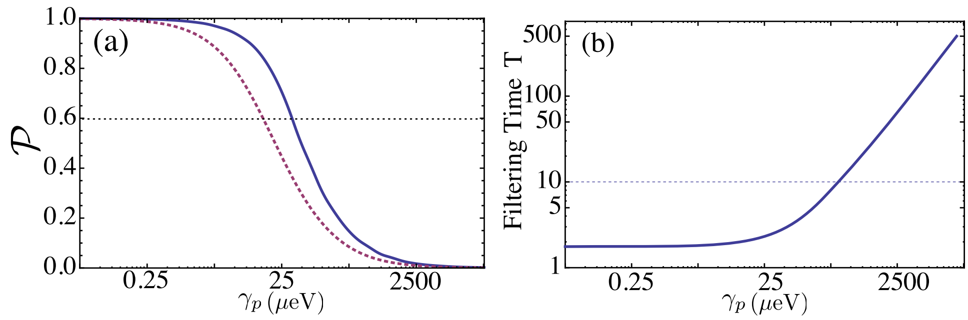

Figure 3.12: (a) Dependences of the purity on γ_p. g, κ and $\omega_d - \omega_c$ are fixed ($g = 25$ μeV, $\kappa = 50$ μeV $\omega_d - \omega_c = 0$). The solid and dotted line are the purity with time filtering ($T = 2/g$ and the fixed efficiency $\mathcal{P}_d = 0.5$) and without time filtering, respectively. (b) Dependences of the corresponding filtering time T on γ_p.

3.5 Summary

We analyzed radiative decay of an excited dot in a solid-state cavity QED system and investigated the quantum-mechanical properties of the emitted photon, stressing the effects of pure dephasing. Our analysis is based on a model in which all the elements of the system (including environmental ones) are treated as active quantum-mechanical degrees of freedom. We rigorously solved the time evolution of the overall system, and derived analytical expressions for the density matrix, pulse shape, spectrum, and purity of the emitted photon. These analytical results were visualized under realistic parameters. The main results are summarized as follows: (i) Changes in the dot decay rate due to pure dephasing can be explained in terms of quantum Zeno and anti-Zeno effects. The emitted photon pulse length is approximately given by the inverse of the dot decay rate. (ii) The emitted photon spectrum agrees with the Glauber formula. The mean energy of an emitted photon is not necessarily identical to that of the dot and energy conservation is seemingly broken. However, the present analysis revealed that the dot can exchange energy with the environment through pure dephasing coupling. Energy conservation holds when the environmental energy is included. (iii) The purity of the emitted photon is calculated as a measure of indistinguishability. The purity is approximately determined by the product of the pure dephasing rate and excitation lifetime before leaving the cavity. When the pure dephasing rate γ_p is fixed, the optimum condition for maximizing the purity is $\omega_d = \omega_c$ and $\kappa \sim g$. (iv) Effects of time filtering are discussed. The purity is improved by filtering out photons emitted later. In actual experiments, the optimum filtering time will depend on to what extent we can permit a lowered efficiency.

Appendix 3.A Relation between coincidence probability and purity

Here we prove the relation $P_{co} = (1 - \mathcal{P})/2$ between the coincidence probability P_{co} and the purity $\mathcal{P}$. We consider the following situation (see Fig. 3.4). Two solid-state emitters (S_1 and S_2) respectively emit single photons simultaneously and deterministically (assuming $\gamma = 0$ for simplicity) into two input ports (P_1 and P_2) of a beamsplitter. These two photons are mixed by the beamsplitter and are output into the ports (P_3 and P_4). We denote the photon field operators for the port P_j by $\widetilde{b}_{(j)r}$ ($j = 1, \cdots, 4$), and the pure-dephasing reservoir operators for the emitter S_j by $\widetilde{d}_{(j)r}$ ($j = 1, 2$). Assuming $t \to \infty$ and $\gamma = 0$ (and therefore $\delta_m = 0$) in Eq. (3.13), the state vector of P_1 photon is given by

$$|\psi_1\rangle = \sum_{m=0}^{\infty} \int drd^m\boldsymbol{x}\gamma_m(t, r, \boldsymbol{x})\widetilde{b}^\dagger_{(1)r}|\boldsymbol{x}\rangle, \tag{3.55}$$

where $|\boldsymbol{x}\rangle = \widetilde{d}^\dagger_{(1)x_1} \cdots \widetilde{d}^\dagger_{(1)x_m}|0\rangle$. Thus, the emitted photon is entangled with the environment of its source. The input state vector including both P_1 and P_2 photons is then given by

$$|\psi_{12}\rangle = \sum_{m,n=0}^{\infty} \int drdr'd^m\boldsymbol{x}d^n\boldsymbol{x}'\ \gamma_m(t, r, \boldsymbol{x})\gamma_n(t, r', \boldsymbol{x}')\widetilde{b}^\dagger_{(1)r}\widetilde{b}^\dagger_{(2)r'}|\boldsymbol{x}; \boldsymbol{x}'\rangle, \tag{3.56}$$

where $|\boldsymbol{x}; \boldsymbol{x}'\rangle = \widetilde{d}^\dagger_{(1)x_1} \cdots \widetilde{d}^\dagger_{(1)x_m}\widetilde{d}^\dagger_{(2)x'_1} \cdots \widetilde{d}^\dagger_{(2)x'_n}|0\rangle$.

The beamsplitter mixes two photons as $\widetilde{b}^\dagger_{(1)r} \to [\widetilde{b}^\dagger_{(3)r} + \widetilde{b}^\dagger_{(4)r}]/\sqrt{2}$ and $\widetilde{b}^\dagger_{(2)r} \to [\widetilde{b}^\dagger_{(3)r} - \widetilde{b}^\dagger_{(4)r}]/\sqrt{2}$, but obviously does not affect the environmental degrees of freedom. Then, the output state vector is given by $|\psi_{out}\rangle = |\psi_{33}\rangle + |\psi_{44}\rangle + |\psi_{34}\rangle$, where

$$|\psi_{33}\rangle = \sum_{m,n=0}^{\infty} \int drdr'd^m\boldsymbol{x}d^n\boldsymbol{x}' \frac{\gamma_m(t,r,\boldsymbol{x})\gamma_n(t,r',\boldsymbol{x}')}{2} \widetilde{b}^\dagger_{(3)r}\widetilde{b}^\dagger_{(3)r'}|\boldsymbol{x};\boldsymbol{x}'\rangle, \tag{3.57}$$

$$|\psi_{44}\rangle = -\sum_{m,n=0}^{\infty} \int drdr'd^m\boldsymbol{x}d^n\boldsymbol{x}' \frac{\gamma_m(t,r,\boldsymbol{x})\gamma_n(t,r',\boldsymbol{x}')}{2} \widetilde{b}^\dagger_{(4)r}\widetilde{b}^\dagger_{(4)r'}|\boldsymbol{x};\boldsymbol{x}'\rangle, \tag{3.58}$$

$$|\psi_{34}\rangle = \sum_{m,n=0}^{\infty} \int drdr'd^m\boldsymbol{x}d^n\boldsymbol{x}' \frac{\gamma_m(t,r,\boldsymbol{x})\gamma_n(t,r',\boldsymbol{x}') - \gamma_m(t,r',\boldsymbol{x})\gamma_n(t,r,\boldsymbol{x}')}{2} \widetilde{b}^\dagger_{(3)r}\widetilde{b}^\dagger_{(4)r'}|\boldsymbol{x};\boldsymbol{x}'\rangle. \tag{3.59}$$

It is readily confirmed that $\langle\psi_{33}|\psi_{33}\rangle + \langle\psi_{44}|\psi_{44}\rangle + \langle\psi_{34}|\psi_{34}\rangle = 1$ and $\langle\psi_{33}|\psi_{33}\rangle = \langle\psi_{44}|\psi_{44}\rangle$. The coincidence probability P_{co}, namely, the probability to find single photons in both ports 3 and 4, is given by $P_{co} = \langle\psi_{34}|\psi_{34}\rangle$. Since the density matrix element is given by

$$\rho(r,r',t) = \sum_{m=0}^{\infty} \int d^m\boldsymbol{x}\gamma^*_m(r',\boldsymbol{x},t)\gamma_m(r,\boldsymbol{x},t), \tag{3.60}$$

P_{co} is recast into the following form:

$$P_{11} = \frac{1}{2} - \frac{1}{2}\int drdr'\rho(r,r',t)\rho(r',r,t) = \frac{1-\mathcal{P}}{2}. \tag{3.61}$$

When pure dephasing is present, the purity of the emitted photon becomes less than unity and the coincidence probability becomes nonzero.

Appendix 3.B Proof of Eqs. (3.50) and (3.51)

Here we analytically evaluate $E_p = \int dk\, k\langle b^\dagger_k(t)b_k(t)\rangle_i$ and $E_e = \int dk\, k\langle d^\dagger_k(t)d_k(t)\rangle_i$ in the $t \to \infty$ limit, where $\langle\cdots\rangle_i = \langle\psi_i|\cdots|\psi_i\rangle$. Switching to the real-space representations, we have

$$E_p = \frac{i}{2}\int dr \left\langle (\partial_r\widetilde{b}^\dagger_r)\widetilde{b}_r - \widetilde{b}^\dagger_r(\partial_r\widetilde{b}^\dagger_r) \right\rangle_i, \tag{3.62}$$

$$E_e = \frac{i}{2}\int dr \left\langle (\partial_r\widetilde{d}^\dagger_r)\widetilde{d}_r - \widetilde{d}^\dagger_r(\partial_r\widetilde{d}^\dagger_r) \right\rangle_i. \tag{3.63}$$

We can confirm from Eq. (3.8) that $\langle(\partial_r b_r^\dagger)b_r\rangle_i = -\kappa\theta(t-\tau)\theta(\tau)\langle(\frac{d}{d\tau}a^\dagger)a\rangle_i$, where $\tau = t - r$. Using similar equations, we have

$$E_p = -\frac{i\kappa}{2}\int_0^\infty d\tau \left\langle(\tfrac{d}{d\tau}a^\dagger)a - a^\dagger(\tfrac{d}{d\tau}a)\right\rangle_i, \tag{3.64}$$

$$E_e = -i\gamma_p\int_0^\infty d\tau \left\langle(\tfrac{d}{d\tau}\sigma^\dagger\sigma)\sigma^\dagger\sigma - \sigma^\dagger\sigma(\tfrac{d}{d\tau}\sigma^\dagger\sigma)\right\rangle_i. \tag{3.65}$$

Using Eqs. (3.11), (3.12) and their conjugates, we have

$$E_p = \kappa\omega_c\int_0^\infty d\tau\langle a^\dagger a\rangle + \frac{g\kappa}{2}\int_0^\infty d\tau\left(\langle a^\dagger\sigma\rangle + \langle\sigma^\dagger a\rangle\right), \tag{3.66}$$

$$E_e = g\gamma_p\int_0^\infty d\tau\left(\langle a^\dagger\sigma\rangle + \langle\sigma^\dagger a\rangle\right). \tag{3.67}$$

Thus, we need to evaluate $I_1 = \int_0^\infty d\tau\langle\sigma^\dagger\sigma\rangle$, $I_2 = \int_0^\infty d\tau\langle a^\dagger a\rangle$, and $I_3 = \int_0^\infty d\tau\langle\sigma^\dagger a\rangle$.

The equations of motion for $\langle\sigma^\dagger\sigma\rangle$, $\langle a^\dagger a\rangle$, and $\langle\sigma^\dagger a\rangle$ are given by

$$\frac{d}{dt}\langle\sigma^\dagger\sigma\rangle = -\gamma\langle\sigma^\dagger\sigma\rangle - ig(\langle\sigma^\dagger a\rangle - c.c.), \tag{3.68}$$

$$\frac{d}{dt}\langle a^\dagger a\rangle = -\kappa\langle a^\dagger a\rangle + ig(\langle\sigma^\dagger a\rangle - c.c.), \tag{3.69}$$

$$\frac{d}{dt}\langle\sigma^\dagger a\rangle = i(\widetilde{\omega}_d^* - \widetilde{\omega}_c)\langle\sigma^\dagger a\rangle + ig(\langle a^\dagger a\rangle - \langle\sigma^\dagger\sigma\rangle). \tag{3.70}$$

Integrating these equations with respect to τ, we have $1 = \gamma I_1 + ig(I_3 - I_3^*)$, $0 = \kappa I_2 - ig(I_3 - I_3^*)$, $0 = i(\widetilde{\omega}_d^* - \widetilde{\omega}_c)I_3 + ig(I_2 - I_1)$. When $\gamma = 0$, these equations are solved to yield $I_2 = 1/\kappa$ and $I_3 = (i/g)\times(\widetilde{\omega}_c^* - \widetilde{\omega}_d)/(\widetilde{\omega}_c + \widetilde{\omega}_d - \widetilde{\omega}_c^* - \widetilde{\omega}_d^*)$. Since $E_p = \kappa\omega_c I_2 + (g\kappa/2)(I_3 + I_3^*)$ and $E_e = g\gamma_p(I_3 + I_3^*)$, we obtain Eqs. (3.50) and (3.51).

Chapter 4

Single-Electron Generator

4.1 Introduction

On-demand coherent single electron source is a promising candidate for transport of quantum information with mobile electrons [79]. For actual application, however, we have to evaluate effect of strong Coulomb interaction between a mobile electron and background (environment) electrons, and to make efforts for reducing its dephaing effect. Whereas dephasing effect due to environment noise has been studied by a simple phenomenological model so far [88, 89], there is no theoretical study to clarify effect of Coulomb interaction between electrons.

In this chapter, we consider dephasing effect in single-electron generation caused by environment noise to a quantum dot, and by Coulomb interaction between electrons. The former calculation is almost the same as the one for single-photon generation, and is helpful to understand dephasing process on electrons. For the latter calculation, we employ a powerful diagrammatic method of the Keldysh type [105, 106]. We show that the present problem is closely related to the so-called *Fermi-edge singularity*, which originates from anomalous edge effect in X-ray absorption [107, 108, 109, 110, 111]. We note that dephasing effect to quantum states of a *localized* electron in a quantum dot has been studied to explain strange nonequilibrium effect in the Mach-Zehnder interferometer made by edge channels of the IQH state [112, 113, 114].

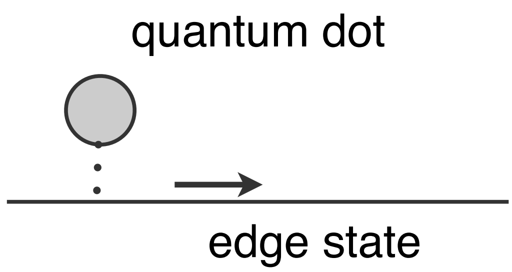

Figure 4.1: A model of single electron generator.

This chapter is organized as follows. We investigate quantum nature of emitted electrons under dephasing effect. We first calculate survival probabilities, spectra, and purities of injected electrons under environment noise in Sec. 4.2. Next, we calculate them under dephasing caused by Coulomb interaction in Sec. 4.3. We finally summarize the results in Sec. 4.4.

4.2 Pure dephasing due to environment noise

4.2.1 Model

Our model consists of a quantum dot connected to a chiral edge mode in IQH states illustrated in Fig. 4.1, and is described by the Hamiltonian

$$\mathcal{H}_0 = \mathcal{H}_{\rm dot} + \mathcal{H}_{\rm edge} + \mathcal{H}_{\rm t}, \tag{4.1}$$

$$\mathcal{H}_{\rm dot} = \epsilon_d d^\dagger d, \tag{4.2}$$

$$\mathcal{H}_{\rm edge} = \int dkka_k^\dagger a_k, \tag{4.3}$$

$$\mathcal{H}_{\rm t} = g(\tilde{a}_0^\dagger d + d^\dagger \tilde{a}_0), \tag{4.4}$$

where $\mathcal{H}_{\rm dot}$, $\mathcal{H}_{\rm edge}$, and $\mathcal{H}_{\rm t}$ express a quantum dot, a one-dimensional chiral edge channel, and tunneling between a dot and a edge channel at the origin. Here, ϵ_d is an energy level of a quantum dot, g is a tunneling amplitude between the quantum dot and the one-dimensional chiral edge state, the wavenumber k of the edge state is measured from the

Fermi wavenember, and the Fermi velocity is set to be unity. The level broadening is given as $\Gamma = g^2$ in this unit.

We consider the Hamiltonian $\mathcal{H} = \mathcal{H}_0 + \mathcal{H}_{\text{env}}$, where the latter denotes effect of environment noise. Here, we employ a simple model for environment noise by using an additional one-dimensional bosonic port as

$$\mathcal{H}_{\text{env}} = \int dk \left[k c_k^\dagger c_k + \sqrt{\gamma_p/\pi} d^\dagger d (c_k^\dagger + c_k) \right], \tag{4.5}$$

where γ_p is a pure dephasing rate.

4.2.2 Result

Under the condition $\Gamma \ll \epsilon_d$, we can calculate analytically the survival probability $P_1(t) = \langle \psi(t) | d_1^\dagger d_1 | \psi(t) \rangle$, the density matrix of emitted electrons $\rho(r, r', t) = \langle \psi(t) | b_{r'}^\dagger b_r | \psi(t) \rangle$, the pulse profile $f(r, t) = \rho(r, r, t)$, the spectrum $S(k, t) = \int dr \int dr' e^{-\mathrm{i}k(r-r')} \rho(r, r', t)$, and the purity $\mathcal{P}(T) = \int dr \int dr' \rho(r, r', t) \rho(r', r, T) / (\int dr \rho(r, r, T))^2$ (including to time-filtering effect by looking at electrons emitted during $0 < t < T$) in the same way of Chap. 3. The results are given as

$$P_1(t) = e^{-\Gamma t}, \tag{4.6}$$

$$\rho(r, r', t) = \Gamma e^{-(i\epsilon_d + \Gamma/2 + \gamma_p)(r'-r) - \Gamma(t-r')}, \quad (r < r'), \tag{4.7}$$

$$f(r, t) = \Gamma e^{-\Gamma(t-r)}, \tag{4.8}$$

$$S(k, t) = \frac{1}{\pi} \frac{\Gamma/2 + \gamma_p}{(k - \epsilon_d)^2 + (\Gamma/2 + \gamma_p)^2}, \tag{4.9}$$

$$\mathcal{P}(T) = \frac{2\Gamma^2}{\Gamma + 2\gamma_p} \left[\frac{1 - e^{-2\Gamma T}}{2\Gamma} - \frac{e^{-\Gamma T - 2\gamma_p T} - e^{-2\Gamma T}}{\Gamma - 2\gamma_p} \right] / \left(1 - e^{-\Gamma T}\right)^2. \tag{4.10}$$

We note that $\rho(r, r\prime, t)$ for $(r > r')$ is obtained by the symmetric relation $\rho(r, r', t) = \rho^*(r', r, t)$. We stress that the pulse profile, which has been measured in experiment of single electron generation by average current, is not affected by pure dephasing rate γ_p. In other words, we cannot get information of pure dephasing from the pulse profile. The spectrum becomes a Lorenzian form with a peak at $k = \epsilon_d$. The peak width is given as $\Gamma + 2\gamma_p$, and is increased by introduction of pure dephasing. It is clear that the emitted electron is not Fourier-limited in the presence the pure dephasing as observed in calculation of Chap. 3.

For no time filtering ($T \to \infty$), the purity, which is a direct measure of coherence in two-particle interferometer, is given as

$$\mathcal{P} \equiv \mathcal{P}(T \to \infty) = \frac{1}{1 + 2\gamma_p/\Gamma}. \tag{4.11}$$

The purity monotonically varies from 1 to 0 as γ_p increases from 0 to ∞. This is a main result for the case of environment noise.

Effect of time filtering is discussed in parallel to the one for single photon generation. Efficiency of the filtering are independent of pure dephasing rate, and filtering time T for a fixed efficiency η is explicitly derived as

$$T = \frac{-1}{\Gamma} \log \left[1 - \sqrt{\eta}\right]. \tag{4.12}$$

The purity is improved as Eq. (4.10) by time filtering paying a cost of reduction of efficiency.

4.3 Effect of Coulomb Interaction

4.3.1 Model

Next, we investigate effect of pure dephasing caused by Coulomb interaction. The Hamiltonian for Coulomb interaction is taken as

$$\mathcal{H}_{\mathrm{C}} = U d^\dagger d \tilde{a}_0^\dagger \tilde{a}_0, \tag{4.13}$$

where U is a local (screened) Coulomb interaction between an electron in a dot and electrons in a edge channel at the origin.

If we focus on electrons in the edge channel, its Hamiltonian changes depending on whether an electron in the dot is emitted into a edge channel or not. We define the Hamiltonian of the edge channel for the empty dot ($n_d = 0$) and the filled dot ($n_d = 1$) as

$$h_0 = \epsilon_d d^\dagger d + \int dk k a_k^\dagger a_k, \tag{4.14}$$

$$h_1 = \epsilon_d d^\dagger d + \int dk k a_k^\dagger a_k + U \tilde{a}_0^\dagger \tilde{a}_0. \tag{4.15}$$

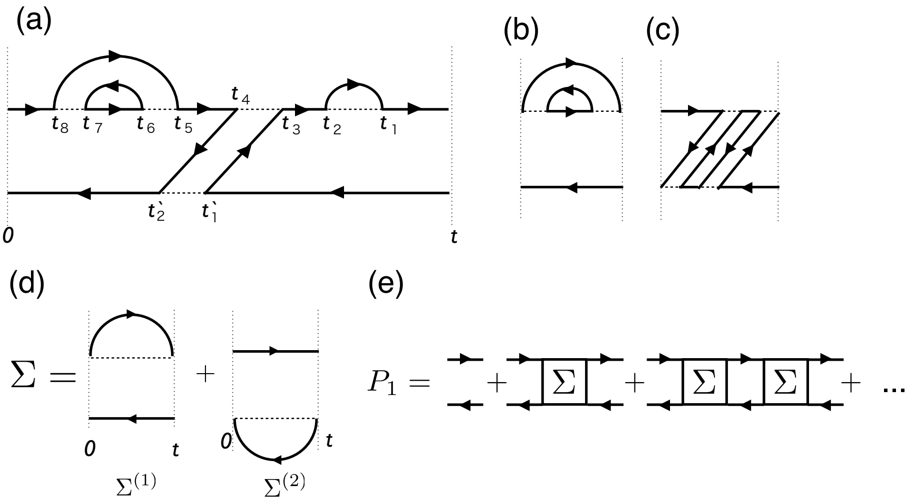

Figure 4.2: (a) Examples of diagrams ($n = 8, n' = 2$); (b)(c) the diagrams representing high energy process neglected in the present calculation; (d) a diagram of the self-energy $\Sigma(t)$; (e) Dyson equation for the survival probability.

Since we assumed local interaction, the effect of the Coulomb interaction can be expressed by the phase shift of electrons in the edge channel. We assume that electrons gain a phase $-\delta$ if the dot is filled ($n_d = 1$), where $\delta > 0$ for repulsive interaction ($U > 0$).

4.3.2 Method

In order to treat Coulomb interaction, we develop a field-theoretical method. The essence of our method is to express a arbitrary observable in the following form

$$\begin{aligned} \langle O(t) \rangle = \int_{t_1 > \cdots > t_n, t_1' > \cdots > t_{n'}}^{t} & dt_1 \cdots dt_n dt_1' \cdots dt_{n'}' \\ & \left\langle \psi(0) \right| \mathcal{V}(t_{n'}') \cdots \mathcal{V}(t_1') O \mathcal{V}(t_1) \cdots \mathcal{V}(t_n) \left| \psi(0) \right\rangle \end{aligned} \tag{4.16}$$

as in a usual procedure deriving Keldysh Green's functions [105, 106]. Here, $\mathcal{V}$ is a interaction representation of the tunneling Hamiltonian $\mathcal{H}_{\rm t}$. Fig. 4.2 (a) shows an example of diagrams. The horizontal two straight lines represent a state of a dot, and the other lines present a electron propagating in the edge channel. In the present calculation, we only treat the leading term for small tunneling amplitude g, and neglect diagrams such as Fig.4.2 (b) and (c) because they describe high energy processes [106].

The survival probability $P_1(t)$ and the decay probability $P_0(t) = 1 - P_1(t)$ are formulated by the sum of diagrams under a constraint that both of the dot states in the upper and lower horizontal line ends the state $n_d = 1$ and $n_d = 0$, respectively. When we define the lowest-order self-energy $\Sigma(t)$ as shown in Fig. 4.2 (d), the survival probability $P_0(t)$ is calculated from the Dyson equation shown in Fig. 4.2 (e). It is convenient to employ the Laplace transform to sum up diagrams appearing the Dyson equation. The final result of the Laplace transformation of $P_1(t)$ and $P_0(t)$ are given as

$$P_1(\lambda) \equiv \int_0^\infty e^{-\lambda t} P_1(t) = \frac{1}{\lambda - \Sigma(\lambda)}, \tag{4.17}$$

$$P_0(\lambda) \equiv \int_0^\infty e^{-\lambda t} P_0(t) = \frac{-\Sigma(\lambda)/\lambda}{\lambda - \Sigma(\lambda)}. \tag{4.18}$$

In a similar way, the density matrix $\rho(k, \bar{k}, t)$ is formulated by the sum of diagrams under a constraint that an electron with a wavelength k and a hole with a wavelength $\bar{k}$ ends at a time t.

First, we consider the survival probability $P_1(t)$. In the leading contribution for small g, the self-energy $\Sigma(t)$ is calculated as

$$\Sigma(t) = 2\mathrm{Re}\left[(-ig)^2 e^{i\epsilon_d t}\left\langle e^{ih_1 t}\tilde{a}_0^\dagger e^{-ih_0 t}\tilde{a}_0\right\rangle_0\right], \tag{4.19}$$

where $\langle \cdots \rangle_0 = \frac{1}{Z}\left[\rho_0 \cdots\right]$, $Z = \mathrm{tr}\rho_0$, and $\rho_0 = e^{-\beta\epsilon}$ is a density matrix at initial state which we here take as a product state of a filled dot ($n_d = 1$) and a Fermi sea at zero temperature. To calculate this average, we adopt the method in Refs. [115, 116, 117]. We first define an operator $\hat{w}$ in the single-particle Hilbert space by

$$\rho_0 e^{\mathrm{i}h_1 t} e^{-\mathrm{i}h_0 t} = \frac{1}{Z}\exp\left(\sum_{k,k'} w_{k,k'} a_k^\dagger a_k\right). \tag{4.20}$$

By using a relation $a_k e^{-ih_1 t} = e^{-ih_1 t} a_k e^{-ikt}$ and the determinant formula derived recently [115], the average in the self-energy is calculated as

$$\Sigma(t) = -2g^2 \mathrm{Re}\left[e^{-i(k-\epsilon_d)t} \int dk d\bar{k} \det(\hat{1} + e^{\hat{w}})(\hat{1} + e^{-\hat{w}})^{-1}_{k\bar{k}} \right], \tag{4.21}$$

The determinant and the inverse $(\hat{1}+e^{-\hat{w}})_{k\bar{k}}$ can be calculated by Riemann-Hilbert factorization in energy domain [117]. Performing the integral respect to $\bar{k}$, we obtain the self energy as

$$\Sigma(t) = -2g^2 \mathrm{Re}\left[e^{i\epsilon_d t} L(t) D(t) \right], \tag{4.22}$$

$$L(t) = \int \frac{dk}{2\pi}(1 - n(k)) \left(\frac{-\xi_0}{k + i\eta} \right)^{2a} e^{-ikt}, \tag{4.23}$$

$$D(t) = (-i\xi_0 t)^{-a^2}, \tag{4.24}$$

where ξ_0 is high energy cutoff and a is a normalized phase shift $a = \delta/\pi$, η is a low-energy cutoff appearing in the Riemann-Hilbert factorization, and $n(k)$ is the Fermi distribution function at zero temperature. We note that L and D represent open and closed diagrams in the work by Nozieres and de Dominicis, respectively [108]. The Laplace transform of $\Sigma(t)$ is then given by

$$\Sigma(\lambda) \equiv \int dt e^{-\lambda t} \Sigma(t) \tag{4.25}$$

$$= -\frac{g^2}{\pi} \Gamma(1-2a)\Gamma(2a - a^2) \mathrm{Im}\left[e^{2i\pi a} \left(\frac{\xi}{\epsilon_d + i\lambda} \right)^{a^2 - 2a} \right], \tag{4.26}$$

where $\Gamma(x)$ is the Gamma function.

Next, we consider density matrix of emitted electrons. To calculate density matrix $\rho(k, \bar{k}, t)$, the self-energies defined by the diagrams in Fig.4.3 (a) are needed. For example, $\Sigma^{(1A)}_{k\bar{k}}$ is given by

$$\Sigma^{(1A)}_{k\bar{k}} = \int \frac{dk' dk''}{(2\pi)^2} \int_0^t d\tau (-ig)(ig) e^{i\epsilon_d \tau} \left\langle e^{ih_1 \tau} a_{k''} e^{ih_0 (t-\tau)} a^\dagger_{\bar{k}} a_k e^{-ih_0 t} a^\dagger_{k'} \right\rangle_0 \tag{4.27}$$

$$= \int \frac{dk' dk''}{(2\pi)^2} \int_0^t d\tau g^2 e^{i\epsilon_d \tau - ik'' \tau - i(k-\bar{k})t} \left\langle e^{\hat{w}} a_{k''} a^\dagger_{\bar{k}} a_k a^\dagger_{k'} \right\rangle_0 \tag{4.28}$$

$$= \int \frac{dk' dk''}{(2\pi)^2} \int_0^t d\tau g^2 e^{i\epsilon_d \tau - ik'' \tau - i(k-\bar{k})t} \det(\hat{1} + e^{\hat{w}})(\hat{1} + e^{\hat{w}})^{-1}_{k''\bar{k}} (\hat{1} + e^{\hat{w}})^{-1}_{kk'} \tag{4.29}$$

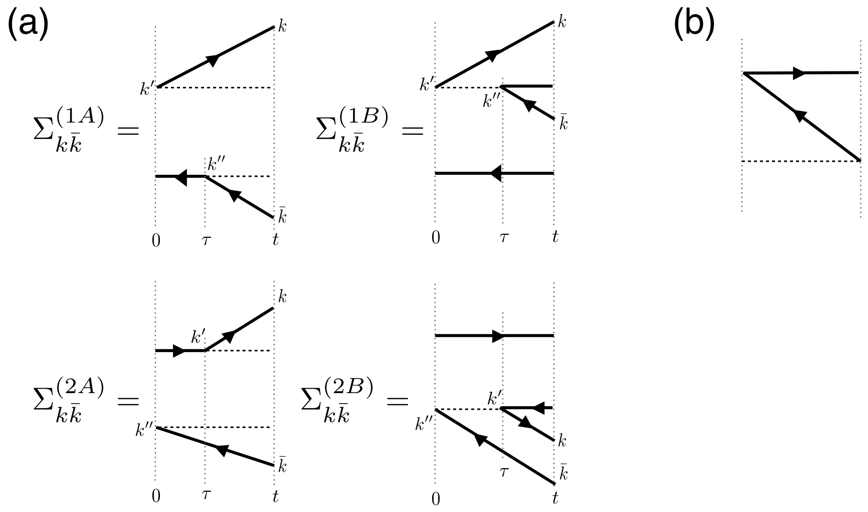

Figure 4.3: diagrams of $\Sigma_{k\bar{k}}$

In a similar way,

$$\Sigma^{(1B)}_{k\bar{k}} = \int \frac{dk'dk''}{(2\pi)^2} \int_0^t d\tau g^2 e^{i\epsilon_d \tau - ik''\tau - i(k-\bar{k})t} \det(\hat{1} + e^{\hat{w}})(\hat{1} + e^{-\hat{w}})^{-1}_{k''\bar{k}}(\hat{1} + e^{\hat{w}})^{-1}_{kk'} \tag{4.30}$$

Using a relation $(\hat{1} + e^{\hat{w}})^{-1}_{k''\bar{k}} + (\hat{1} + e^{-\hat{w}})^{-1}_{k''\bar{k}} = \delta_{k''\bar{k}}$, we obtain

$$\Sigma^{(1)}_{k\bar{k}} \equiv \Sigma^{(1A)}_{k\bar{k}} + \Sigma^{(1B)}_{k\bar{k}} \tag{4.31}$$

$$= \int \frac{dk'}{(2\pi)^2} \int_0^t d\tau g^2 e^{i\epsilon_d \tau - i\bar{k}\tau - i(k-\bar{k})t} \det(\hat{1} + e^{\hat{w}})(\hat{1} + e^{\hat{w}})^{-1}_{kk'} \tag{4.32}$$

The Laplace transform of $\Sigma^{(1)}_{k\bar{k}}$ is derived as

$$\Sigma^{(1)}_{k\bar{k}}(\lambda) = \int dt e^{-\lambda t} \Sigma^{(1)}_{k\bar{k}}(t) \tag{4.33}$$

$$= i\frac{g^2}{\xi_0}\Gamma(1-a^2)\left(\frac{\xi_0}{k+i\eta}\right)^{2a} \frac{1}{\lambda + i(k-\bar{k})} \left(\frac{\xi_0}{\epsilon_d - k + i\lambda}\right)^{1-a^2} \tag{4.34}$$

$\Sigma^{(2)}_{k\bar{k}}$ is obtained by complex conjugate of $\Sigma^{(2)}_{\bar{k}k}$.

We mention that hole excitation in edge state ($k < 0$) does not contribute the density matrix at all. This is because that the sign of the phase shift is opposite to electrons due to attractive interaction. For the attractive scattering, singular behavior due to the Fermi surface effect is much more weak, and can be shown to be small in comparison with contribution from electrons.

The density matrix of emitted electron is obtained by

$$\rho(k,\bar{k},\lambda) = \frac{\Sigma_{k\bar{k}}(\lambda)}{\lambda - \Sigma(\lambda)} \tag{4.35}$$

In order to asymptotic behavior of the spectrum ($t \to \infty$), we multiply λ and take a limit $\lambda \to 0$ and $k \to \bar{k}$. The spectrum can be written as

$$\begin{aligned} S(k) &= 2\mathrm{Re}[\Lambda_{kk}]/(-\Sigma(0)) \qquad (4.36)\\ &= \frac{-2g^2}{(-\Sigma(0))\xi_0}\Gamma(1-a^2)\mathrm{Im}\left[\left(\frac{\xi_0}{k+i\eta}\right)^{2a}\left(\frac{\xi_0}{i\eta-(k-\epsilon_d)}\right)^{1-a^2}\right], \qquad (4.37)\\ &= \frac{2g^2}{(-\Sigma(0))\xi_0}\Gamma(1-a^2)\sin\phi\left(\frac{\xi_0}{k^2+\eta^2}\right)^{a}\left(\frac{\xi_0}{(\epsilon_d-k)^2+\eta^2}\right)^{\frac{1-a^2}{2}}, \qquad (4.38)\\ \phi &= 2a\tan^{-1}\frac{\eta}{k} + (1-a^2)\tan^{-1}\frac{\eta}{\epsilon_d - k}. \qquad (4.39) \end{aligned}$$

where $\Lambda_{k\bar{k}} \equiv \lim_{\lambda\to 0}\lambda\Sigma_{k\bar{k}}$ and $-\Sigma(0)$ behaves as a normalization factor of the spectrum. We can check the following sum rule:

$$\int \frac{dk}{2\pi}\Sigma_{kk}(\lambda) = \frac{-\Sigma(\lambda)/\lambda}{\lambda - \Sigma(\lambda)}. \tag{4.40}$$

This relation guarantee that the sum of the spectrum of emitted electrons is equal to the decay probability $P_0(t)(= 1 - P_1(t))$.

Fig. 4.4 shows the spectrum of emitted electrons. If the phase shift is small enough, the spectrum is Lorentzian which peak is at ϵ_d. With increasing the phase shift, a singular peak near the Fermi sea grows up, and the main peak at ϵ_d change its form into asymmetric one. We note that the small peak near the Fermi sea is caused by closed loop contribution in Nozieres's work, whereas the growth of the peak near the Fermi sea indicate degrade of the purity of the emitted electrons.

Finally, we evaluate the purity. We define $\tilde{\rho}(\lambda) = \rho(\lambda + i(\bar{k} - k))$ and $\tilde{\Sigma}(\lambda) = \Sigma(\lambda + i(\bar{k} - k))$ to take the time dependence for sufficiently large t.

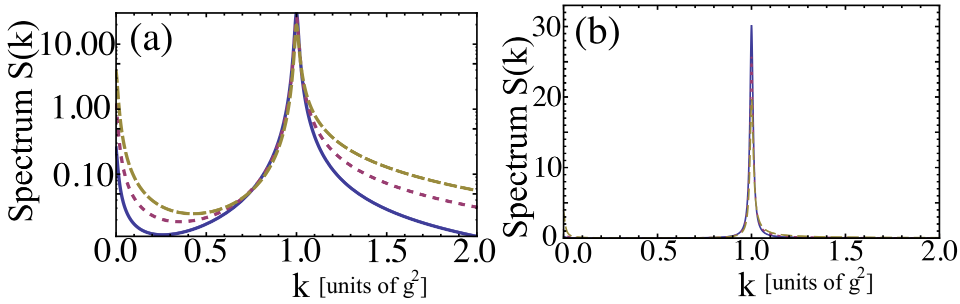

Figure 4.4: (a) A linear plot and (b) a log plot of spectrum $S(k)$. Parameters are taken as $\epsilon_d = g^2$, $\eta = 0.01g^2$, and the phase shift is taken as $a = \delta/\pi =$ 0.1 (solid), 0.2 (dotted), and 0.3 (dashed).

We obtain $\tilde{\rho}(\lambda)$ as

$$\tilde{\rho}(\lambda) = \frac{\frac{g}{\xi_0}\Gamma(1-a^2)/\lambda}{-i\lambda + \bar{k} - k + i\tilde{\Sigma}} \left[\left(\frac{\xi_0}{k+i\eta}\right)^{2a} \left(\frac{\xi_0}{\epsilon_d - \bar{k} + i\lambda}\right)^{1-a^2} - \left(\frac{\xi_0}{\bar{k}-i\eta}\right)^{2a} \left(\frac{\xi_0}{\epsilon_d - k - i\lambda}\right)^{1-a^2} \right], \tag{4.41}$$

Asymptotic behavior of $\tilde{\rho}$ in $t \to \infty$ is derived by $\lim_{\lambda\to 0} \lambda\tilde{\rho}(\lambda)$, which has singular points at $k = \bar{k}$ and $\bar{k} - k + i\Sigma(0) = 0$. If we can neglect latter term, the purity is finally written as

$$\mathcal{P} = \int \frac{dkd\bar{k}}{(2\pi)^2} \rho(k,\bar{k})\rho(\bar{k},k) \tag{4.42}$$

$$= \frac{1}{(4\pi B(1-2a, 2a-a^2)\sin(2a\pi))^2} \int dxd\bar{x} \frac{\Sigma(0)^2}{(x-\bar{x})^2 + \Sigma(0)^2} \times \left| \frac{1}{(x+i\eta)^{2a}(1-\bar{x}+i\eta)^{1-a^2}} - \frac{1}{(\bar{x}-i\eta)^{2a}(1-x-i\eta)^{1-a^2}} \right|^2 \tag{4.43}$$

This is a main result for dephasing caused by Coulomb interaction.

4.4 Summary

We have discussed dephasing effect on quantum coherence of single electrons injected from a quantum dot. We have shown that environment noise does not change the spatial profile of emitted electrons, whereas the spectrum and the purity is affected by pure dephasing due to the environment. For dephasing caused by Coulomb interaction, we have obtained a singular behavior in the spectrum of emitted electrons. This singular behavior originates from the Fermi surface effect, which is famous as a name of the Fermi edge singularity. We expect that this singular change of quantum nature in emitted electrons strongly affect the degrade of the purity.

Chapter 5

Shot Noise and Fractional Statistics

This chapter is organized as follows. After breif introduction in Sec. 5.1, let us start with our model in Sec.5.2. An operator of quasi-particles in the edge states is constructed by bosonization techniques of Hamiltonian representing incompressible liquids. In Sec.5.3, non-equilibrium Kubo formula in mesoscopic systems is introduced to define shot noise at finite temperatures. In Sec.5.4, we discuss Fano factor (normalized shot noise) and propose a way to indirectly obtain statistical angle in hierarchical FQH states.

5.1 Introduction

The fractional quantum Hall (FQH) effect occurs in the two dimensional electron system subject to a strong magnetic field. A confining geometry in low disorder samples makes the edges gapless modes, which carries fractionally charged quasi-particles. The quasi-particles are characterized by exotic features of fractional charge and fractional statistics. The fractional statistics is determined by a phase gained by adiabatic exchange process of quasi-particles. The direct observation of these properties has been a stimulating problem. The fractional charge has been observed both well by many of shot noise measurements[18, 19, 20, 120, 121, 122], which is now the well-established scheme.

Fractional statistics is also appealing and mutual statistics has been measured. Other attempts were made in Ref.[124], and Refs.[125, 126] where cross-correlation in three edge states was studied for the Laughlin states at zero temperature. Kim extended their works into hierarchical FQH states at finite frequency and temperature, and then discussed statistics for $\nu = 1/5,\ 2/5$ [95]. It is well known that quasi-particles in $\nu = 1/5,\ 2/5$ FQH states have the same charge, but obey different statistics. Shot noise measurement in the low-temperature limit succeeded to confirm the former [120], but failed to do the latter. Ref.[95] gave an idea to the problem, but not realized in experiments. We revert back to the standard set up, and discuss shot noise in two edge states instead of three ones. What is most important point is that finite temperature effects are considered on the basis of a recent work [127]. It is shown that the approach enables us to detect the difference of statistics in $\nu = 1/5,\ 2/5$ FQH states. Finally we discuss a method to determine statistical angle itself in hierarchical FQH states.

This chapter is organized as follows. Let us start with our model in Sec.5.2. An operator of quasi-particles in the edge states is constructed by bosonization techniques of Hamiltonian representing incompressible liquids. In Sec.5.3, non-equilibrium Kubo formula in mesoscopic systems is introduced to define shot noise at finite temperatures. In Sec.5.4, we discuss Fano factor (normalized shot noise) and propose a way to indirectly obtain statistical angle in hierarchical FQH states.

5.2 Model and method

Fractional quantum hall liquid has energy gap in bulk states due to Coulomb interaction and it is incompressible. In a system with confining geometry, edge states exist to satisfy gauge invariance. Canonical quantization of Hamiltonian representing density excitation at edges leads that the density operator obeys Kac-Moody algebra. By making appropriate bosonic operators from the density operators, it is shown that the edge states can be written as chiral Tomonaga-Luttinger liquid. Oper-

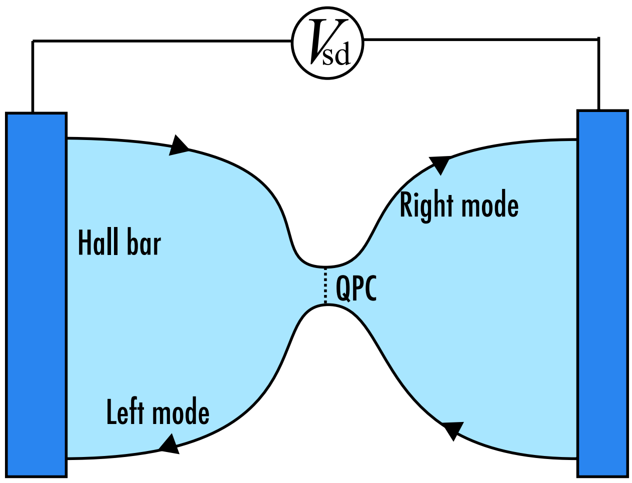

Figure 5.1: Schematic illustration of setup to detect shot noise.

ators for electrons and quasi-particles can be composed and condition from electrons' anti-commutation relation shows that the quasi-particles are of IQHE or Laughlin's FQHE states.

Let us consider the quasi-particle tunneling through the QPC set at $x = 0$ between edge states[18, 131, 72]. The gapless edge states are described by chiral Tomonaga-Luttinger liquids. We begin with Laughlin states with filling fractions $\nu = 1/(2n+1)$ for simplicity. The Hamiltonian is given by right/left going edge modes H_R, H_L and the tunneling part H_B:

$$H = H_R + H_L + H_B \tag{5.1}$$

$$H_{R,L} = \frac{v_F}{\pi}\int_{-\infty}^{\infty} dx \left(\frac{\partial\phi_{R,L}(x)}{\partial x}\right)^2, \tag{5.2}$$

$$H_B = t_B\psi_R^\dagger(0)\psi_L(0) + h.c., \tag{5.3}$$

where we put Planck constant $\hbar$ one, v_F is the Fermi velocity, t_B is the tunneling amplitude of quasi-particles, $\phi_{R,L}(x)$ are chiral boson fields. The density operator obeys the U(1) Kac-Moody algebra. The operator for electron can be composed by imposing that the electron obeys the anti-commutation relation. However, the same procedure cannot give the operator for quasi-particle because it obeys a different statistics. Wen introduced a duality transformation: $\nu \to 1/\nu$, and thus $\psi_{R,L}(x)$ represent the vertex operators in $c = 1$ CFT as

$$\psi_{R,L}(x) = \frac{1}{\sqrt{2\pi}} e^{\pm ik_F x} : e^{\mp i\sqrt{\nu}\phi_{R,L}(x)} : . \tag{5.4}$$

This construction is also available for hierarchical Laughlin's states with K-matrix. K-matrix allows us to write the condition for a filling factor to make hierarchical states. In such a filling factor, edge states have multi modes naively. A mode with the maximum exponent carries charge current and other modes are charge neutral. If we neglect charge neutral modes, we can construct an operator of quasi-particles by replace ν to an exponent α. In this study, we neglect charge neutral modes, however, there is a theoretical work which states the charge neutral modes becomes relevant at especially low temperature. We discuss later in this relation.

The quasi-particle hopping with an unit charge e^* generates backscattering current:

$$\hat{I}_B \equiv ie^* \left(e^{i\omega_0 t} t_B \psi_R^\dagger(0)\psi_L(0) - e^{-i\omega_0 t} t_B^* \psi_L^\dagger(0)\psi_R(0) \right) . \tag{5.5}$$

Following the discussion of a gauge transformation [72], source-drain bias voltage V is incorporated into phase factor $\omega_0 = e^* V$. The backscattering current and current noise are obtained as

$$I_B = \left\langle \hat{I}_B(t) \right\rangle , \qquad S = \int dt' \left\langle \left\{ \delta\hat{I}_B(t), \delta\hat{I}_B(t') \right\} \right\rangle .$$

These quantities can be calculated on the basis of Schwinger-Keldysh formalism(Appendix 5.B).

5.3 Non-equilibrium Kubo formula

In this section, let us introduce shot noise at finite temperatures, proposed in the context of a generalization from the Kubo formula: non-equlibrium Kubo Formula.

5.3.1 Landauer formula

First, we start with a non-interacting case such as $\nu = 1$. In this case, Landauer formula is correct and charge current I_B^0 and its noise S^0 can be written as

$$I_B^0 = e \int \frac{d\omega}{\pi} T_0(f_L - f_R), \tag{5.6}$$

$$\begin{aligned} S^0 &= e^2 \int \frac{d\omega}{\pi} T_0 \left[f_L(1-f_L) + f_R(1-f_R) \right] \\ &= e^2 \int \frac{d\omega}{\pi} T_0 \left[(f_L - f_R)^2 \right], \end{aligned} \tag{5.7}$$

where f_L and f_R are Fermi distribution functions of left and right reservoirs and transmission probability $T_0 = |t_B|^2/v_F^2$. At zero temperature, thermal noise vanishes in the first line of Eq. 5.7. The second line of Eq. 5.7 clearly originates from non-equilibrium nature, called as shot noise in Landauer formula. At finite temperatures, shot noise separates from thermal noise. Thus it enables us to investigate shot noise in view of thermal fluctuation.

5.3.2 Interacting case

Next, we turn to the discussion about interacting case. It is well known that for correlated electrons Landauer formula is not satisfied in principle. At zero temperature, thermal noise must vanish and non-equilibrium shot noise can be defined without any problems. However, correlation effects generally merge thermal noise and shot noise at finite temperatures**??**(Eq.5.48). interactions mix bias voltage dependence of thermal noise and non-equilibrium noise at finite temperature. Thus, there is arbitrariness about definition of shot noise. It is a problem what a kind of thermal noise at finite temperature should be subtracted from total noise and shot noise.

5.3.3 Non-equilibrium Kubo formula

It is well known that the standard Kubo formula determines linear conductance. In contrast, a relation to differential conductance G under finite bias voltages were derived [127]. Thus this formula was called as the nonequilibrium Kubo formula in mesoscopic systems. This formula is valid for any quantum transport systems with two reservoirs whose Hamiltonian is described by

$$H = H_L + H_R + H_c + H_{cL} + H_{cR}. \tag{5.8}$$

H_L and H_R describes left/right reservoirs connected to finite conductor H_c H_{cL} and H_{cR} describes couplings between the left/right reservoirs and the conductor. The formula can be applied to various systems, including quantum dots, quantum point contacts, and chiral Luttinger liquids on the quantum Hall edge. Then, it was also proposed to define shot noise at any temperature S_h as the following formula:

$$S_h \equiv -\langle\{\delta I, e(\delta N_L - \delta N_R\}\rangle\,, \tag{5.9}$$

where $\delta A \equiv A - \langle A\rangle$. I and $N_{L,R}$ are the charge current and number of particles in left/right reservoirs. It was proved that S_h in eq.(5.9) has several aspects expected as shot noise. (i) In a non-interacting system, S_h directly gives the Landauer-type shot noise at finite temperatures. (ii) At zero temperature, S_h is agreement with the standard shot noise: current noise S at $T = 0$. (iii) In the linear response regime, $S_h = 0$ and eq.(5.10) reproduces the Nyquist-Johnson relation. As a result S_h is qualified as shot noise at finite temperatures. Actually using S_h it was successful to study shot noise of the Kondo effect in a quantum dot [128, 129, 130]. In this study, we apply the formula to the system represented by 5.1, replacing I and e Eq. 5.9 to I_B and e^* respectively.

The nonequilibrium Kubo formula also satisfies the relation:

$$S_h = S - 4k_BTG, \tag{5.10}$$

where S is current noise, $G = \partial_V I_B$ is differential conductance, k_B is Boltzmann constant, and T is temperature in reservoirs. This relation shows us what variations of thermal noise should be subtracted from current noise to define shot noise at finite temperatures in experiments. Our framework gives a prospective way to study shot noise at finite temperatures: S_h in eq.(5.9) is directly calculated, and its prediction is examined through $S - 4k_{\mathrm{B}}TG$ in experiments. In the following the approach is applied to edge states.

5.4 Results and discussions

In this section, we discuss shot noise and fano factor at finite temperature. When we show the graphs for specific parameters, we are taking an unit of $|t_B|^2/v_F^2 = 1$.

5.4.1 Current and Current Noise

Conventionally information on a fractional charge is extracted from Poisson noise. Thus, when the quasi-particle weakly transmits through the QPC, it is sufficient to calculate these transport quantities up to the lowest order $O(t_B^2)$. These expressions can be rewritten into Landauer forms:

$$I_B = e^* \int \frac{d\omega}{2\pi} T(\omega)(f_L - f_R), \tag{5.11}$$

$$\begin{aligned} S &= e^{*2} \int \frac{d\omega}{\pi} T(\omega)(f_L(1-f_L) + f_R(1-f_R)) \\ &\quad + e^{*2} \int \frac{d\omega}{\pi} T(\omega)(f_L - f_R)^2. \end{aligned} \tag{5.12}$$

The transmission probability is characterized by the t-matrix $t(\omega) \equiv \pi t_B \rho(\omega)$:

$$\begin{aligned} T(\omega) &\equiv t^*(\omega - \omega_0/2)\, t(\omega + \omega_0/2), \\ \rho(\omega) &= \frac{t_B}{v_F} \cosh\left(\frac{\beta\omega}{2}\right) \left(\frac{2\pi}{\beta v_F}\right)^{\nu-1} \frac{|\Gamma\left(\frac{\nu}{2} + i\frac{\beta\omega}{2\pi}\right)|^2}{\pi\Gamma(\nu)}. \end{aligned} \tag{5.13}$$

Here $\rho(\omega) \equiv -\mathrm{Im}G^r(\omega)/\pi$ is the density of states (DOS) at $x = 0$ and $G^r(\omega)$ is retarded Green's function at $x = 0$. Figure 5.2 shows the ω-dependence of transmission probability for $\nu = 1, 1/3, 1/5$ for $V = 1, 2$. In the $\nu = 1$ IQH state or non-interacting edge states, $T(\omega)$ in eq.(5.13) leads to a constant $|t_B|^2/v_F^2$ and remains unchanged when a bias voltage is tuned.

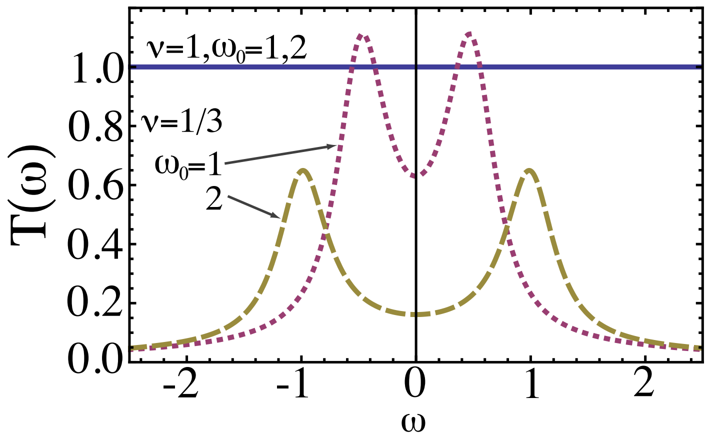

Figure 5.2: Energy dependence of density of states $\rho(\omega)$ for $\nu = 1, 1/3, 1/5$ and $\beta = 1$.

When electrons are non-interacting ($\nu = 1$), the density of states are constant. However, when Coulomb interactions are turned on ($\nu = 1/3$), $T(\omega)$ has double peaks at chemical potentials: $\omega = \pm\omega_0/2 = \pm e^* V/2$.

In the $\nu = 1$ IQH state or non-interacting edge states, $T(\omega)$ in eq.(5.13) leads to a constant $|t_B|^2$. Within our approximation, only the transmission probability is renormalized by Coulomb interaction through the DOS. In contrast the Fermi distribution function is unrenormalized as

$$f_{L,R} \equiv \frac{1}{1 + \exp(\beta(\omega \pm \omega_0/2))}. \tag{5.14}$$

5.4.2 Fano factor and peak structure

Seemingly, the second line in eq.(5.12) might be interpreted as shot noise in view of a Landauer-formula sense. However, shot noise formula in eq.(5.9) modifies the naive prediction. Following the same approximation, eq.(5.9) can be calculated, and rewritten into a Landauer-like form:

$$S_h = S_L + \delta S_L, \tag{5.15}$$
$$S_L = e^{*2} \int \frac{d\omega}{\pi} T(\omega)(f_L - f_R)^2,$$
$$\delta S_L = e^{*2} \int \frac{d\omega}{\pi} T(\omega)(f_L - f_R)(y_L - y_R), \tag{5.16}$$

where S_L represents a Landauer-type shot noise and δS_L does the correction term. Here,

$$y(\omega) \equiv \frac{1}{2}\tanh\left(\frac{\beta\omega}{2}\right) - \frac{1}{\pi}\mathrm{Im}\left[\Psi\left(\frac{\nu}{2} + i\frac{\beta\omega}{2\pi}\right)\right],$$
$$y_{L,R} \equiv y\left(\omega \pm \omega_0/2\right), \tag{5.17}$$

where $\Psi(z)$ is the digamma function. In case of $\nu = 1$, because $\delta S_L = 0$ and $T(\omega) = |t_B|^2/v_F^2$, it is exemplified that S_h is equivalent to the Landauer-type shot noise S_L for $\nu = 1$ at finite temperatures. Thus the correction term δS_L plays an essential role in FQH states.

Let us discuss the feature in view of the nonequilibrium Kubo formula. $G = \partial_V I_B$ is calculated using eq.(5.11), and then the resulting G and S are substituted into $S - 4k_B TG$. Therefore, we confirm that the result is identical with S_h in eq.(5.15), so that the nonequilibrium Kubo formula eq.(5.10) is satisfied. In the context it is found that δS_L corresponds to the V-derivative of $T(\omega)$. As shown in Fig.5.2, $T(\omega)$ depends on V.

To proceed a further discussion, we introduce the following Fano factor:

$$F_\nu \equiv \frac{S_h}{2e^* I_B}. \tag{5.18}$$

The different point compared to a standard Fano factor is to be normalized by an unit charge e^*. In the low-temperature/high-bias limit, $S_h/2I_B$ converges to e^*, as discussed later. With the normalization factor at zero temperature, it enables us to focus on thermal fluctuation of shot noise. Here in Fig.5.3 F_ν for $\nu = 1/3$ at a fixed inverse temperature $\beta = 1$ is compared to $F_{L\nu}$ and $\delta F_{L\nu}$ defined by

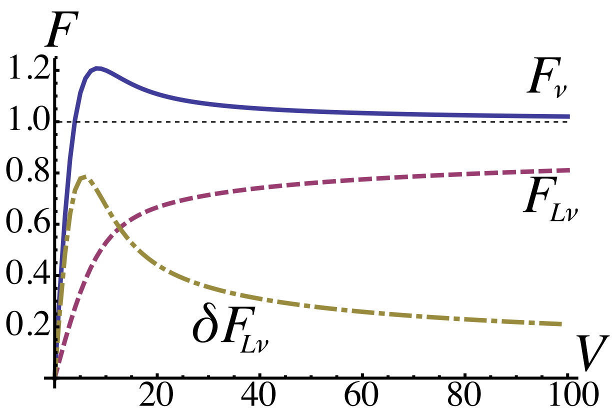

Figure 5.3: Bias dependence of F_ν (solid line), $F_{L\nu}$ (dashed line) and $\delta F_{L\nu}$ (dashed-dotted line) for $\nu = 1/3$ at $\beta = 1$

$$F_{L\nu} \equiv \frac{S_L}{2e^* I_B}, \tag{5.19}$$

$$\delta F_{L\nu} \equiv \frac{\delta S_L}{2e^* I_B}. \tag{5.20}$$

$F_{L\nu}$ monotonously changes, on the other hand $\delta F_{L\nu}$ exhibits non-monotonous behavior with increasing bias voltage V. The total Fano factor F_ν which is the sum of them converges to 1 in the high-bias limit. The fact represents that the charge of the quasiparticle is e^* because F_ν is normalized by the unit charge. In contrast, we find the peak structure at a finite bias which originates from the correction noise $\delta F_{L\nu}$.

If we regard the Fano factor as an effective charge function, it turns out that the enhancement from the unit charge occurs. Transmitted quasi-particles are seemed to tend to come together due to thermal fluctuation. The peak structure is a sign for carried charges to bunch induced by thermal fluctuation. Therefore we call the effect "*thermal bunching*". Note that this "*thermal bunching*" is different from the bunching which originates from statistics of quasi-particles [95].

Fig.5.4(a) shows F_ν at a fixed $\nu = 1/3$ for several inverse temperatures β. As lowering temperature, a peak position moves to a lower bias. What

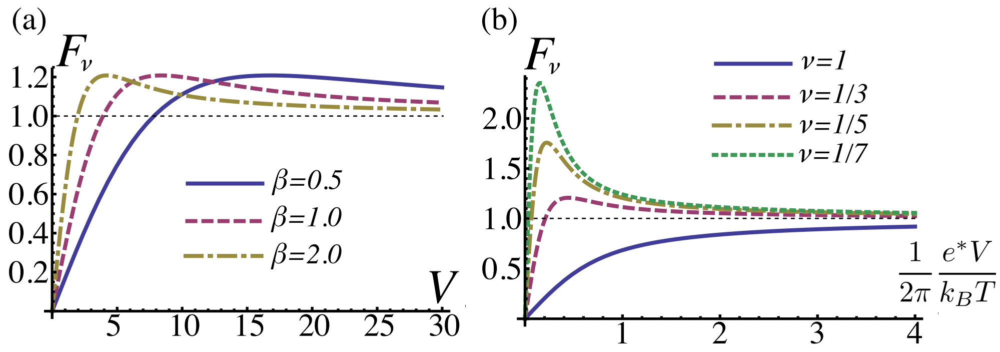

Figure 5.4: (a) F_ν for $\beta = 0.5, 1.0, 2.0$ at $\nu = 1/3$ (solid line, dashed line, dash-dotted line); (b) F_ν for $\nu = 1, 1/3, 1/5, 1/7$ at $\beta = 1$ (solid line, dashed line, dash-dotted line, dotted line)

is universal nature is that the peak height is unchanged. On the other hand in Fig.5.4(b) F_ν at a fixed $\beta = 1$ is drawn for some parameters ν. The peak structure does not appear in the $\nu = 1$ IQH state. The peak height becomes larger for smaller ν, namely, stronger magnetic field or Coulomb interaction. Figure 5.5(a) shows filling factor dependence of the peak height. We find that the peak height diverges in the limit of $\nu \to 0$ as,

$$\lim_{\nu\to+0} F_\nu|_{\max} \to \frac{1}{\pi\nu}, \tag{5.21}$$

and the right hand side approximates well even with finite fillings. Figure 5.5(b) shows filling factor dependence of the peak position $y \equiv \frac{1}{2\pi}\frac{e^*V}{k_BT}$. As easily seen, the peak position is equal to the filling factor in the limit of $\nu \to 0$.

Up to now, our discussion has been restricted to Laughlin states with $\nu = 1/(2n+1)$. As said in the introduction, we would like to consider statistics for $\nu = 1/5,\ 2/5$. Here thus we extend our discussion into hierarchical FQH states (ex.$\nu = 2/5, 3/7, 2/9, \cdots$). Those states are characterized by filling fraction, unit charge and statistical angle:

$$\nu = \frac{p}{2np+1} \quad e^* = e\frac{1}{2np+1} \quad \theta = \pi\frac{2n(p-1)+1}{2np+1} \tag{5.22}$$

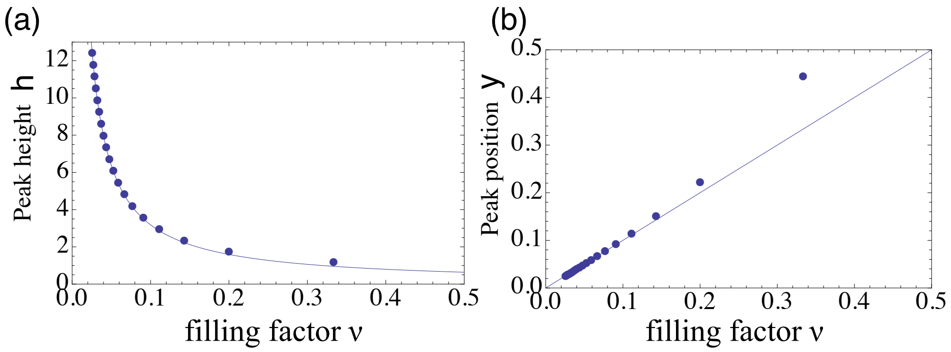

Figure 5.5: (a) Dots shows dependence of the peak height h of the Fano factor F_ν on the filling factor $\nu = 1/(1+2n)$ and the solid line shows $h = 1/\pi\nu$. (b) Dots shows dependence of the peak position $y = \frac{1}{2\pi}\frac{e^*V}{k_BT}$ of the Fano factor F_ν on the filling factor $\nu = 1/(1+2n)$ and the solid line shows $y = \nu$.

which are originally defined through the K-matrix [131, 132] and n and p are positive integer. Our formalism developed above is described by the quasi-particle Green function at $x = 0$. This treatment can be also justified when multiple tunneling processes can be neglected (discuss later). Thus the extension changes the exponent ν to α in eq.(5.29):

$$\alpha = \frac{1}{p(2np+1)}. \tag{5.23}$$

Furthermore, the current eq.(5.11), current noise eq.(5.12) and shot noise eq.(5.15) have been expressed as a frequency-integral form, in accordance with the concept of Landauer formula. Concerning the current and current noise, integrated results were derived for Laughlin states[72]. According to the same idea, shot noise can be also calculated. The result is straightforwardly extended into hierarchical FQH states, and thus the Fano factor is governed by a scaling function:

$$F_\alpha = \frac{2}{\pi}\mathrm{Im}\left[\Psi\left(\alpha + i\frac{1}{2\pi}\left(\frac{e^*V}{k_BT}\right)\right)\right]. \tag{5.24}$$

This function is characterized by exponent α.

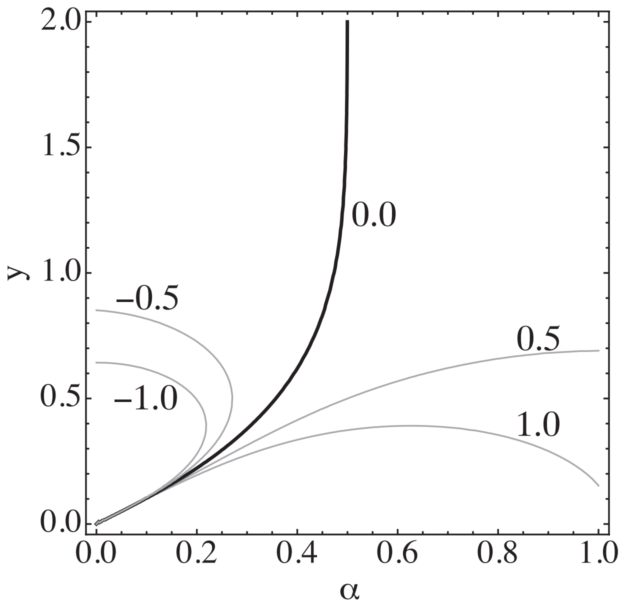

Figure 5.6: Contour plot of differential Fano factor $\partial_V F_\alpha$=-1.0,-0.5,0,0.5,1.0. The thick line shows $\partial_V F_\alpha = 0$.

Taking advantage of the scaling form, let us reexamine the peak structure of the Fano factor. We plot $\partial_V F_\alpha$ taking α as a continuous parameter(Fig.5.6). It is found that $\alpha < 1/2$ is the sufficient condition for emergence of peak. It is easily shown that $\alpha = 1/p(2np + 1)$ is less than 1/2, and thus the peak structure develops in all type of hierarchical FQH states represented by Eq.(5.22).

5.4.3 Discussion

As an experimentally relevant case, let us discuss statistics in FQH states with $\nu = 1/5$, $2/5$. The quantities listed in eq.(5.22) are specifically obtained for these states:

$\nu = 1/5$	$e^*_{1/5} = e/5$	$\theta_{1/5} = \pi/5$	$(n, p) = (2, 1)$
$\nu = 2/5$	$e^*_{2/5} = e/5$	$\theta_{2/5} = 3\pi/5$	$(n, p) = (1, 2)$

As mentioned in the introduction, $e^*_{1/5} = e^*_{2/5} = e/5$ has been confirmed through shot noise measurement in the low-temperature limit[120]. However, there still remain the problem on statistics.

To address the issue we begin with generic relations among e^*,θ,ν and α in eqs.(5.22) and (5.23). Each of e^*,θ,ν and α is determined by two integer parameters: n and p. Thus the independent quantities become two of them, and others are given by them. Therefore the statistical angle discussed here is represented in all type of hierarchical FQH states as

$$\theta = \pi \left[1 - \alpha \left(\frac{e}{e^*} - 1 \right) \right]. \tag{5.25}$$

The result yields one-on-one relations between α and θ using $e^*_{1/5} = e^*_{2/5} = e/5$:

$$\alpha_{1/5} = \frac{1}{4}\left(1 - \frac{\theta_{1/5}}{\pi}\right),\ \alpha_{2/5} = \frac{1}{4}\left(1 - \frac{\theta_{2/5}}{\pi}\right). \tag{5.26}$$

In conclusion, in order to see the difference of statistical angles there is a way to discuss exponents α.

We substitute $\alpha_{1/5}$, $\alpha_{2/5}$ in eq.(5.26) into eq.(5.24) for $\nu = 1/5,\ 2/5$ respectively, and show the Fano factors for $\nu = 1/5,\ 2/5$ in Fig.(5.7). In the low-temperature/high-bias limit, both Fano factors converge to 1. This is a generic feature of the Fano factor normalized by unit charge e^*. In the present case for $\nu = 1/5,\ 2/5$, even if the normalization by e is considered, the limiting values are equal: $e^*_{1/5}/e = e^*_{2/5}/e = 1/5$. It turns out that shot noise in the low-temperature/high-bias limit cannot distinguish statistics. What is striking is that the Fano factors of $\nu = 1/5, 2/5$ have difference at finite temperature/bias. The Fano factor is determined by observable quantities thruogh eq.(5.10) and (5.18). Analyzing its Fano factor, it is possible to distinguish statistics of $\theta_{1/5}$ and $\theta_{2/5}$ in experiments.

The estimation of exponent α has been already reported by analyzing the power-law dependence of tunneling current: $I \propto V^{\alpha}$[21]. Our approach makes it possible to obtain both α and e^* in the shot noise measurement with the scaling function which does not contain non-universal parameters eq.(5.24) .

In this study, we discuss Fano factor defined by shot noise. It is difficult to subtract thermal noise at finite temperature appropriately. Then, there is a naive question, "Why we need non-equilibrium noise?

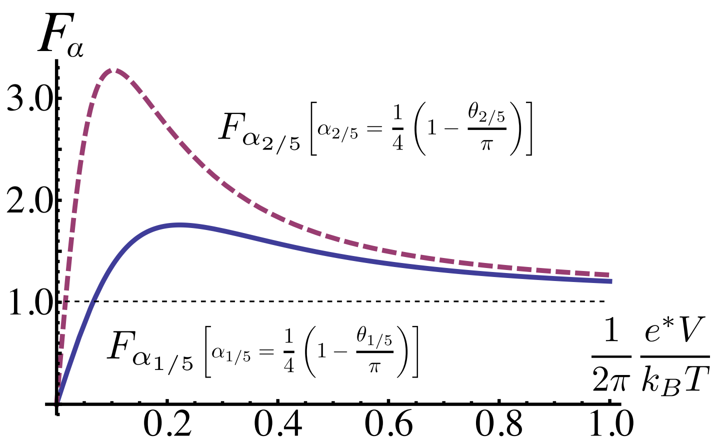

Figure 5.7: Fano factors of $\nu = 1/5$ (Laughlin state) and $\nu = 2/5$ (hierarchical FQH state). Both quasi-particles have the same fractional charge $e/5$.

Isn't the current noise power S sufficient?" To clarify this, a Fano factor defined as a ratio between total current noise S and backscattering current I_B is,

$$\frac{S}{2e^* I_B} = \coth(\omega_0\beta/2), \tag{5.27}$$

and it does not include α. A subtle additional problem with this ratio is diverging at $V \to 0$ limit. Our shot noise does not diverge for any bias voltages.

Finally we comment on a closely-related work by Ferarro et al.[133]. They pointed out that the tunneling is dominated by multiple particles at $T < T^*$, in contrast the single particle at $T > T^*$. The dynamics of neutral edge mode determines the crossover temperature T^*, evaluated as 50mK in the experiment[134]. Thus our treatment, which has focused on the single-particle process, still stands in the region of $T > T^*$.

5.5 Summary

In summary the finite-temperature shot noise at FQH edge states has been studied on the basis of the nonequilibrium Kubo formula. The peak structure of Fano factor has been found at a bias voltage. We have named the phenomena "thermal bunching" because this is a sign for quasi-particles to weakly glue, mediated by thermal fluctuation. The phenomena has been determined by a scaling function characterized by an exponent of quasi-particle Green function. In $\nu = 1/5,\ 2/5$ FQH states, exponents have been given by only statistical angles. Detecting the discrepancy of Fano factors, one can measure the difference of statistics. Finally we have proposed an indirect way to determine a statistical angle from exponent fitted to the scaling function and unit charge estimated at sufficiently low temperature within $T > T^*$

Appendix 5.A Keldysh Green's function

The quasi-particle Green's function is defined by

$$G^{\eta_1\eta_2}_{R,L}(x,t) \equiv -i\left\langle T_K \psi_{R,L}(x,t^{\eta_1})\psi^\dagger_{R,L}(0,0^{\eta_2})\right\rangle . \tag{5.28}$$

Under the Hamiltonian(Eq. 5.1), this correlations can be calculated. The greater and lesser part of Green function are

$$G^{\pm\mp}_{R,L}(x,t) = \frac{\pm i}{2\pi}\left(\frac{i\frac{\pi}{\beta v_F}}{\sinh\frac{\pi}{\beta v_F}(-x+tv_F \pm i\epsilon)}\right)^{\nu}, \tag{5.29}$$

where ϵ is an infinitesimal positive number where $\eta_1, \eta_2 = \pm$ represents a branch of the Keldysh contour. We also define $G^{\pm\mp}_{R,L}(t) \equiv G^{\pm\mp}_{R,L}(0,t)$ to simplify.

These Green's functions satisfy symmetry-like relations,

$$G^{\eta,\bar{\eta}}_{r}(-x,-t) = -G^{\bar{\eta},\eta}_{r}(x,t), \tag{5.30}$$

$$G^{\eta_1,\bar{\eta}}_{r}(-x,-t) = G^{\eta,\bar{\eta}}_{-r}(x,t), \tag{5.31}$$

$$G^{\eta,\bar{\eta}}_{r}(x,t) = G^{\eta,\bar{\eta}}_{-r}(x,-t). \tag{5.32}$$

These relations are alike to "particle-hole symmetry", "parity symmetry" and "time reversal" respectively.

We also define Fourier transformation

$$G(\omega) = \int dt G(t) e^{i\omega t}. \tag{5.33}$$

Appendix 5.B Calcultion of Current and Current Noise Power

In this appendix, we represent backscattering current I_B and current noise power S by Green's functions. These quantity can be written by

$$I_B = \frac{1}{2}\sum_{\eta_1} \left\langle T_K \left\{ \hat{I}_B(t^{\eta_1}) \exp\left(-i\int_K d\tau_1 H_B(\tau_1)\right)\right\}\right\rangle, \tag{5.34}$$

$$S(t,t_1) = \left\langle \hat{I}_B(t)\hat{I}_B(t_1)\right\rangle + \left\langle \hat{I}_B(t_1)\hat{I}_B(t)\right\rangle - 2\left\langle \hat{I}_B(t)\right\rangle\left\langle \hat{I}_B(t_1)\right\rangle, \tag{5.35}$$

$$= \sum_{\eta_1} \left\langle T_K \left\{ \hat{I}_B(t^{\eta_1})\hat{I}_B(t_1^{\bar{\eta}_1}) \exp\left(-i\int_K d\tau_1 H_B(\tau_1)\right)\right\}\right\rangle \tag{5.36}$$

$$S = S(\omega = 0), \tag{5.37}$$

where $\bar{\eta} \equiv -\eta$. We expand these quantity in t_B to second order. The backscattering current is

$$\frac{I_B}{e^*|t_B|^2/2} = \sum_{\eta_1\eta_2\epsilon\epsilon_1} \epsilon\eta_2 \int dt_1 e^{i\epsilon\omega_0 t + i\epsilon_1\omega_0 t_1} \left\langle T_K \left\{ \left[\psi_R^\dagger(t^{\eta_1})\psi_L(t^{\eta_1})\right]^{\epsilon} \left[\psi_R^\dagger(t_1^{\eta_2})\psi_L(t_1^{\eta_2})\right]^{\epsilon_1}\right\}\right\rangle, \tag{5.38}$$

where η_1, η_2 are indices of Keldysh contour($\pm$), $\epsilon, \epsilon_1 = \pm$ and

$$\left[\psi_R^\dagger(t^{\eta_1})\psi_L(t^{\eta_1})\right]^+ \equiv \psi_R^\dagger(t^{\eta_1})\psi_L(t^{\eta_1}) \tag{5.39}$$

$$\left[\psi_R^\dagger(t^{\eta_1})\psi_L(t^{\eta_1})\right]^- \equiv \psi_L^\dagger(t^{\eta_1})\psi_R(t^{\eta_1}). \tag{5.40}$$

Using Wick's theorem, we take apart these correlations into products of Green's functions. Terms such as $\left\langle \psi_L\psi_L\right\rangle$ and $\left\langle \psi_L^\dagger\psi_L^\dagger\right\rangle$ vanishes, so $\epsilon = -\epsilon_1$. Resulting Green's functions only depend on $t - t_1$, so we shall rewrite $t - t_1$ into t.

$$\frac{I_B}{e^*|t_B|^2/2} = \sum_{\eta_1\eta_2} \eta_2 \int dt \left\{ e^{i\omega t} G_R^{\eta_2\eta_1}(-t) G_L^{\eta_1\eta_2}(t) - e^{-i\omega t} G_R^{\eta_1\eta_2}(t) G_L^{\eta_2\eta_1}(-t) \right\}, \tag{5.41}$$

$$= \sum_{\eta_1\eta_2} \int dt (\eta_2 - \eta_1) e^{i\omega_0 t} G_R^{\eta_2\eta_1}(-t) G_L^{\eta_1\eta_2}(t). \tag{5.42}$$

In the last line, we change t to $-t$ and replace η_1 and η_2 of the last term. With help of Eq.5.31, we obtain

$$\frac{I_B}{e^*|t_B|^2} = \sum_{\eta_1} \int dt e^{i\omega_0 t} \eta_1 \left[G_R^{\bar{\eta}_1\eta_1}(-t) \right]^2. \tag{5.43}$$

Similarly, the current noise power S can be represented by Green's functions as

$$\frac{S(t)}{e^{*2}|t_B|^2} = -\sum_{\eta_1} 2\cos(\omega_0 t) \left[G_R^{\bar{\eta}_1\eta_1}(-t) \right]^2, \tag{5.44}$$

$$\frac{S}{e^{*2}|t_B|^2} = \left. \frac{S(\omega)}{e^{*2}|t_B|^2} \right|_{\omega \to 0}, \tag{5.45}$$

$$= -2 \sum_{\eta_1} \int dt \cos(\omega_0 t) \left[G_R^{\bar{\eta}_1\eta_1}(-t) \right]^2. \tag{5.46}$$

These integrals can be performed by replacing $t' = t \mp i\epsilon \pm \beta/2$ [72]. The results are

$$\frac{I_B}{e^*|t_B|^2} = \frac{1}{\pi^2 v_F^{2\nu}} \left(\frac{2\pi}{\beta} \right)^{2\nu-1} \sinh\left(\frac{\omega_0\beta}{2} \right) \left| \Gamma\left(\nu + i\frac{\omega_0\beta}{2\pi} \right) \right|^2 \tag{5.47}$$

$$\frac{S(\omega)}{e^{*2}|t_B|^2} = \frac{2}{\pi^2 v_F^{2\nu}} \left(\frac{2\pi}{\beta} \right)^{2\nu-1} \cosh\left(\frac{\omega_0\beta}{2} \right) \left| \Gamma\left(\nu + i\frac{\omega_0\beta}{2\pi} \right) \right|^2. \tag{5.48}$$

Fourier transformation of the lasser and greater Green's functions are obtained by the same path-integral and we obtain a relation

$$G^{\eta\bar{\eta}}(\omega) = \eta i f^{\eta}(\omega) \rho(\omega). \tag{5.49}$$

Using this relation, we can rewrite Eqs.5.43 and 5.46 into Landauer-like form in Eqs.5.11 and 5.12 by straightforward calculation.

Appendix 5.C Calculation of Shot Noise from Eq.(5.9)

Shot noise defined by non-equilibrium Kubo formula can be calculated from $S_h = S - 4k_BTG$. However, if we calculate S_h from Eq.(5.9), we should care a treatment for $\delta N(t)$. Shot noise is defined by Eq.5.9 and can be written by

$$I_B = -2\sum_{\eta_1}\left\langle T_K\left\{\delta\hat{I}_B(t^{\eta_1})\delta Q(t^{\bar{\eta}_1})\exp\left(-i\int_K d\tau_1 H_B(\tau_1)\right)\right\}\right\rangle, \tag{5.50}$$

$$N(t) = \frac{1}{2}\int dx\left(\mathcal{N}[\psi_R^\dagger(x,t)\psi_R(x,t) - \psi_L^\dagger(x,t)\psi_L(x,t)]\right), \tag{5.51}$$

where $\mathcal{N}$ means normal order. We represent S_h by Green's function, however, scrupulous care should be taken in handling δQ because of the normalization. When applying Wick's theorem, correlations which includes normal ordered terms should be normalized by operator product expansion such as,

$$\begin{aligned}
&\left\langle\mathcal{N}[\psi_R^\dagger(x,t^{\bar{\eta}_1})\psi_R(x,t^{\bar{\eta}_1})]\psi_R^\dagger(0,t^{\eta_1})\psi_R(t,t_1^{\eta_2})\right\rangle && (5.52)\\
&= \frac{-1}{2\pi}\left\langle T_K\partial_x\phi_R(x,t^{\bar{\eta}_1})\psi_R^\dagger(0,t^{\eta_1})\psi_R(t,t_1^{\eta_2})\right\rangle && (5.53)\\
&= -(G_{R0}^{\bar{\eta}_1\eta_2}(x,t-t_1) - G_{R0}^{\bar{\eta}_1\eta_1}(x,0))G_{R0}^{\eta_2\eta_1}(0,t_1-t), && (5.54)
\end{aligned}$$

where G_{r0} is non-interacting Green's function and in the last line we apply operator product expansion. Thus S_h can be written as

$$\begin{aligned}
\frac{S_h}{e^{*2}|t_B|^2} = i\sum_{\eta_1\eta_2}\tau_z^{\eta_2\eta_2}&\int dxdt2\cos(\omega_0 t)G^{\eta_1\eta_2}(t)G^{\eta_2\eta_1}(-t)\\
&\times\sum_r\left(G_{r0}^{\bar{\eta}_1\eta_2}(x,t) - G_{r0}^{\bar{\eta}_1\eta_1}(x,0)\right).
\end{aligned} \tag{5.55}$$

Integration of $G_{r0}^{\bar{\eta}_1\eta_2}(x,t) - G_{r0}^{\bar{\eta}_1\eta_1}(x,0)$ respect to x works as a kernel for integral respect to t. When performing integral respect to t, singularities are relevant, however, above expression is not suitable for extract the singularities. In order to treat the singularities properly, we replace the x depending terms as

$$G_{r0}^{\bar{\eta}_1\eta_2}(x,t) - G_r^{\bar{\eta}_1\eta_1}(x,0) \to -G_{r0}^{\bar{\eta}_1\eta_1}(x,0)G_{r0}^{\eta_2\bar{\eta}_1}(-x,-t)\mathcal{G}_r^{\eta_2\eta_1}(0,-t), \tag{5.56}$$

where $\mathcal{G}_r$ is an pointer of singularities and equal to inverse of G_{r0} near the singularities. To proceed calculation, we use next relations (as shown later),

$$\int dx G^{\bar{\eta}\eta}_{r0}(x,0)G^{\eta\bar{\eta}}_{r0}(-x,t) = \begin{cases} \frac{v_F t}{\beta} G^{-+}_{R0}(0,-t) & (r=R) \\ \frac{v_F t}{\beta} G^{+-}_{R0}(0,-t) & (r=L) \end{cases} \tag{5.57}$$

$$\int dx G^{\bar{\eta}\eta}_{r0}(x,0)G^{\bar{\eta}\bar{\eta}}_{r0}(-x,t) = \begin{cases} \frac{v_F t}{\beta} G^{-+}_{R0}(0,-t) - \theta(t) i\eta G^{\bar{\eta}\eta}_{R0}(0,-t) & (r=R) \\ \frac{v_F t}{\beta} G^{+-}_{R0}(0,-t) - \theta(-t) i\eta G^{\bar{\eta}\eta}_{R0}(0,-t) & (r=L) \end{cases} \tag{5.58}$$

First, we consider a case of $\eta_1 = \eta_2 = \eta$. Using Eqs.(5.57,5.57),

$$\begin{aligned}
&\sum_r \int dx G^{\bar{\eta}\eta}_{r0}(x,0)G^{\eta\bar{\eta}}_{r0}(-x,-t)\mathcal{G}^{\eta\eta}_{r0}(0,-t) \\
&= \frac{v_F t}{\beta}(G^{-+}_{R0}(0,-t) + G^{+-}_{R0}(0,-t)) \times \\
&(\theta(-\eta t)\sinh\frac{\pi}{\beta}(t+i\eta\epsilon) + \theta(\eta t)\sinh\frac{\pi}{\beta}(t-i\eta\epsilon)), \\
&= \frac{v_F t}{\beta}\left[\theta(-\eta t)\left\{\frac{t+i\eta\epsilon}{t+i\epsilon} + \frac{t+i\eta\epsilon}{t-i\epsilon}\right\} + \theta(\eta t)\left\{\frac{t-i\eta\epsilon}{t+i\epsilon} + \frac{t-i\eta\epsilon}{t-i\epsilon}\right\}\right] \\
&= \frac{2v_F t}{\beta}
\end{aligned} \tag{5.59}$$

In these transformations, we picked up singular parts near $\tau = 0$ which survive when we integrate respect to t and used a relation,

$$\frac{x + i\eta_2\epsilon}{x + i\eta_1\epsilon} \to 1 + \frac{\eta_2 - \eta_1}{2} 2\pi i x \delta(x). \tag{5.60}$$

Next, we see a case of $-\eta_1 = \eta_2 = \eta$. In the same way in Eq.(5.59), using Eqs.(5.58), we obtain

$$\sum_r \int dx G^{\bar{\eta}\eta}_{r0}(x,0)G^{\bar{\eta}\bar{\eta}}_{r0}(-x,-t)\mathcal{G}^{\eta\eta}_{r0}(0,-t) = \frac{2v_F t}{\beta} - i\eta \tag{5.61}$$

Eq.(5.55) can be calculated by using Eqs.(5.56,5.59) and (5.61). As easily seen, the part of $\eta_1 = \eta_2 = \eta$ (Eq.5.59) vanishes, because the integrand is odd in τ. Only the part of $-\eta_1 = \eta_2 = \eta$ (Eq.) survives and we obtain

$$\frac{S_h}{e^{*2}|t_B|^2} = i\int dt 2\cos\omega_0 t \frac{-2t}{\beta}\sum_\eta \eta\left(G^{\eta\bar{\eta}}(0,t)\right)^2 - \int dt 2\cos\omega_0 t\sum_\eta \eta\left(G^{\eta\bar{\eta}}(0,t)\right)^2$$
$$= \frac{S}{e^{*2}|t_B|^2} - \frac{4}{\beta e^*}\frac{\partial}{\partial V}\frac{I_B}{e^*|t_B|^2}, \tag{5.62}$$

here we used

$$t\cos\omega_0 t = \frac{\partial}{\partial\omega_0}\sin\omega_0 t = \frac{\partial}{e^*\partial V}\sin\omega_0 t. \tag{5.63}$$

Eq. (5.62) reproduces non-equilibrium Kubo formula $S_h = S - 4k_BTG$.

We prove Eqs.(5.57,5.58). First, we prove of Eq.(5.57). We show the prove only for $r = R$. The left hand side of Eq.(5.57) is

$$\int dx G^{\bar{\eta}\eta}_{R0}(x,0)G^{\eta\bar{\eta}}_{R0}(-x,-t) = \int dx\frac{-1}{(2\pi)^2}g^\eta(x)g^\eta(x - v_Ft), \tag{5.64}$$

where $g^\eta(x)$ is

$$g^\eta(x) \equiv \frac{\frac{\pi}{\beta}}{\sinh\frac{\pi}{\beta}(x + i\eta\epsilon)}. \tag{5.65}$$

We define the Fourier transformation of g as

$$g^\eta(k) = \frac{1}{2\pi}\int dx e^{ikx}g^\eta(x) \tag{5.66}$$
$$= -\eta i f(\eta k), \tag{5.67}$$
$$f(k) = \frac{1}{1 + e^{\beta k}}. \tag{5.68}$$

We substitute Eq.(5.66) to Eq.(5.64).

$$\int dx G^{\bar{\eta}\eta}_{R0}(x,0)G^{\eta\bar{\eta}}_{R0}(-x,-t)$$
$$= \int\frac{dk}{2\pi}f(\eta k)f(-\eta k)e^{-ikv_Ft} \tag{5.69}$$
$$= \frac{-1}{2\pi\beta}\int dk f'(k)e^{-ikv_Ft} \tag{5.70}$$
$$= \frac{-1}{2\pi\beta}\left\{\left[f(k)e^{-ikv_Ft}\right] - \int dk f(k)(-iv_Ft)e^{-ikv_Ft}\right\} \tag{5.71}$$
$$= \frac{v_Ft}{\beta}\int\frac{dk}{2\pi}(-if(k))e^{-ikv_Ft} \tag{5.72}$$
$$= \frac{v_Ft}{\beta}G^{-+}_R(0. - t). \tag{5.73}$$

In Eq.(5.70), we use $f(\eta k)f(-\eta k) = -f'(k)/\beta$.

Next, we prove Eq.(5.58). The left hand side of Eq.(5.58) is

$$\int dx G_{R0}^{\bar{\eta}\eta}(x,0)G_{R0}^{\bar{\eta}\bar{\eta}}(-x,-t) = \theta(-\tau)\int dx \frac{-1}{(2\pi)^2} g^{\eta}(x) g^{\eta}(x - v_F t) \\ + \theta(\tau)\int dx \frac{-1}{(2\pi)^2} g^{-\eta}(x) g^{-\eta}(x - v_F t). \tag{5.74}$$

The first term of the right hand side is equal to $\theta(-t)\times$Eq.(5.57) and the second term is

$$-\theta(t)\int \frac{dk}{2\pi} f(\eta k)^2 e^{-ikv_F t} \tag{5.75}$$

$$= -\eta i\theta(t)\int \frac{dk}{2\pi}(-\eta i f(\eta k))e^{-ikv_F t} - \frac{\theta(t)}{2\pi\beta}\int dk f'(k) e^{-ikv_F t} \tag{5.76}$$

$$= -\eta i\theta(t) G_R^{\bar{\eta}\eta}(0,-t) + \theta(t)\frac{v_F t}{\beta} G_R^{-+}(0,-t) \tag{5.77}$$

In Eq.(5.76), we use a relation $f(\eta k)^2 = f(\eta k) + f'(k)/\beta$. Thus we substitute the Eq.(5.77) to Eq.(5.74) and obtain

$$\int dx G_{R0}^{\bar{\eta}\eta}(x,0)G_{R0}^{\bar{\eta}\bar{\eta}}(-x,-t) = \frac{v_F t}{\beta} G^{-+}(0,-t) - \eta i\theta(t) G_R^{\bar{\eta}\eta}(0,-t). \tag{5.78}$$

Chapter 6

Summary

In this thesis, we have theoretically investigated three subjects related to the Hong-Ou-Mandel-type experiment to characterize statistics of mobile particles. We summarize the results obtained in this thesis as well as problems left for a future study.

In Chap. 3, we have studied dephasing effect on single photon generator made in the semiconductor cavity QED [23]. By employing a simple model with one-dimensional bosonic channel, we have obtained analytical results for quantum nature of photons emitted from single-photon generator. For realistic experimental parameters, we have evaluated survival probabilities, spectra, and purities as a function of various parameters, and have discussed optimal condition for generation of coherent single photons. Preliminary results on improvement of purities by time filtering have also shown. Detailed discussion on effect of various filtering technique, which is useful for realization of excellent single-photon emission for quantum information, is an important future problem. The theoretical treatment of the non-Markovian noise such as $1/f$ noise is also a important problem left for future study to describe superconducting cavity QED systems.

In Chap. 4, we have studied a fermionic analogy of single-photon generation, i.e., single-electron generation into an integer quantum Hall edge state. We have considered dephasing due to level fluctuation and Coulomb interaction between an electron in a quantum dot and electrons in a edge state. In particular for the latter effect, we have derived field-theoretical method to approach this problem including nontrivial Fermi-surface effects such as Anderson orthogonality theorem and the Fermi-edge singularity. We have calculated survival probabilities, spectra, and purities, and have discussed how environment noise and Coulomb interaction with electrons in an edge channel degrades quantum coherence of electrons. For further description in actual single electron generation, finite-temperature effect, coexistence of noise and Coulomb interaction, and dephasing effect on several theoretical proposals for quantum information processing should be studied in more detail, and are left for a future problem.

In Chap. 5, we have studied current and current noise at finite temperatures under weak reflection between two fractional quantum Hall edge states [24]. We have defined an (extended) Fano factor at finite temperatures, and have calculated it for dominant channel of backscattering channel at moderate temperatures for which neutral modes are irrelevant. We have demonstrate that this extended Fano factor is useful to determine a statistical angle, which characterizes the exchange relation between two fractional charge excitations. Extension of this discussion toward non-Abelian statistics followed by quasi-particles of $\nu = 5/2$ fractional quantum Hall states is an important future problem.

Bibliography

[1] M. A. Nielsen and I. L. Chuang, *Quantum Computation and Quantum Information* (Cambridge University Press, Cambridge, 2000).

[2] L. Mandel and E. Wolf, *Quantum Coherence and Quantum Optics* (Cambridge University Press, Cambridge, 1995).

[3] D. Walls and G. J. Milburn, *Quantum Optics* (Springer-Verlag, New York, 1995).

[4] P. R. Berman, *Cavity Quantum Electrodynamics*, (Academic, Boston, 1994).

[5] R. Miller, T. E. Northup, K. M. Birnbaum, A. Boca, A. D. Boozer, and H. J. Kimble, J. Phys. B: At. Mol. Opt. Phys. **38**, S551 (2005).

[6] G. Khitrova, H. M. Gibbs, M. Kira, S. W. Koch, and A. Scherer, Nature Phys. **2**, 81 (2006).

[7] K. von Klitzing, G. Dorda, and M. Pepper, Phys. Rev. Lett. **45**, 494 (1980).

[8] G. Fève, A. Mahé, J. Berroir, T. Kontos, B. Plaçais, D. C. Glattli, A. Cavanna, B. Etienne, Y. Jin, Science **316**, 1169 (2007).

[9] C. K. Hong, Z. Y. Ou, and L. Mandel, Phys. Rev. Lett. **59**, 2044 (1987).

[10] R. Hanbury Brown and R. Q. Twiss, Phi. Mag., Ser. 7 **45**, 663 (1954).

[11] R. Hanbury Brown and R. Q. Twiss, Nature **177**, 27 (1956).

[12] E. Purcell, Nature **178**, 1449 (1956).

[13] R. Hanbury Brown and R. Q. Twiss, Nature **178**, 1046 (1956).

[14] R. Hanbury Brown and R. Q. Twiss, Proc. Royal. Soc. London Ser. A **242**, 300 (1957).

[15] R. Hanbury Brown and R. Q. Twiss, Proc. Royal. Soc. London Ser. A **243**, 291 (1957).

[16] D. C. Tsui, H. L. Stormer, and A. C. Gossard, Phys. Rev. Lett. **48** (1982) 1559.

[17] R. B. Laughlin, Phys. Rev. Lett. **50** (1983) 1395.

[18] C. L. Kane and M. P. A. Fisher, Phys. Rev. Lett. **72**, 724 (1994).

[19] L. Saminadayar, D. C. Glattli, Y. Jin and B. Etienne: Phys. Rev. Lett. **79** (1997) 2526.

[20] R. de-Picciotto, M. Reznikov, M. Heiblum, V. Umansky, Nature **389**, 162 (1997).

[21] A. M. Chang, Rev. Mod. Phys. **75**,1449 (2003).

[22] F. E. Camino, W. Z. Zhou, and V. J. Goldman, Phys. Rev. Lett. **95** 246802 (2005).

[23] E. Iyoda, T. Kato, T. Aoki, K. Edamatsu, and K. Koshino, arXiv:1112.1485.

[24] E. Iyoda and T. Fujii, J. Phys. Soc. Jpn. **80**, 073709 (2011).

[25] E. T. Jaynes and F. W. Jaynes, Proc. IEEE **51**, 89 (1963).

[26] F. W. Cummings, Phys. Rev. **140**, A1051 (1965).

[27] B. Yurke, J. S. Denker, Phys. Rev. A **29**, 1419 (1984).

[28] M. J. Collett and C. W. Gardiner, Phys. Rev. A **30**, 1386 (1984).

[29] C. W. Gardiner, IBM J. Res. Dev. **32**, 127 (1988).

[30] C. W. Gardiner and P. Zoller, *Quantum Noise* (Springer, Berlin, 1991).

[31] Y. He and E. Barkai, Phys. Rev. A **74**, 011803 (2006).

[32] K. Yoshimi and K. Koshino, Phys. Rev. A **82**, 033818 (2010).

[33] P. Michler, A. Kiraz, C. Becher, W. V. Schoenfeld, P. M. Petroff, Lidong Zhang, E. Hu, A. Imamoğlu, Science **290**, 2282 (2000).

[34] C. Santori, M. Pelton, G. Solomon, Y. Dale, and Y. Yamamoto, Phys. Rev. Lett. **86**, 1502 (2001).

[35] G. S. Solomon, M. Pelton, and Y. Yamamoto, Phys. Rev. Lett. **86**, 3903 (2001).

[36] E. Moreau, I. Robert, J. M. Gérard, I. Abram, L. Manin, and V. Thierry-Mieg, App. Phys. Lett. **79**, 2865 (2001).

[37] M. Pelton, C. Santori, J. Vucˇković, , B. Zhang, G. S. Solomon, J. Plant, and Y. Yamamoto, Phys. Rev. Lett. **89**, 233602 (2002).

[38] T. Yoshie, A. Scherer, J. Hendrickson, G. Khitova, H. M. Gibbs, G. Rupper, C. Ell, O. B. Shchekin, D. G. Deppe, Nature **432**, 200 (2004).

[39] J. P. Reithmaler, G. Sęk, A. Löffler, C. Hofmann, S. Kuhn, S. Reizenstein, L. V. Keldysh, V. D. Kulakovskii, T. L. Reinecke, A. Forchel, Nature **432**, 197 (2004).

[40] E. Peter, P. Senellart, D. Martrou, A. Lemaître, J. Hours, J. M. Gérard, and J. Bloch, Phys. Rev. Lett. **95**, 067401 (2005).

[41] S. Strauf, K. Hennessy, M. T. Rakher, Y.-S. Choi, A. Badolato, L. C. Andreani, E. L. Hu, P. M. Petroff, and D. Bouwmeester, Phys. Rev. Lett. **96**, 127404 (2006).

[42] K. Srinivasan and O. Painter, Nature **450**, 862 (2007).

[43] K. Srinivasan and O. Painter, Phys. Rev. A **75**, 023814 (2007).

[44] A. Blais,R.-S. Huang, A. Wallraff, S. M. Girvin, and R. J. Schoelkopf, Phys. Rev. A **69**, 062320 (2004).

[45] A. Wallraff, D. I. Schuster, A. Blais, L. Frunzio, R.-S. Huang, J. Majer, S. Kumar, S. M. Girvin, and R. J. Schoelkopf, Nature **431**, 162 (2004).

[46] A. A. Houck, D. I. Schuster, J. M. Gambetta, J. A. Schreier, B. R. Johnson, J. M. Chow, L. Frunzio, J. Majer, M. H. Devoret, S. M. Girvin, R. J. Schoelkopf, Nature **449**, 328 (2007).

[47] M. Hofheinz, E. M. Weig, M. Ansmann, R. C. Bialczak, E. Lucero, M. Neeley, A. D. O'connell, H. Wang, J. M. Martinis, and A. N. Cleland, Nature **454**, 310 (2008).

[48] M. Hofheinz, H. Wang, M. Ansmann, R. C. Bialczak, E. Lucero, M. Neeley, A. D. O'connell, D. Sank, J. Wenner, J. M. Martinis, A. N. Cleland, Nature **459**, 546 (2009).

[49] A. Clerk, S. Girvin, F. Marquardt, and R. Schoelkopf, Rev. Mod. Phys. **82**, 1155 (2011).

[50] S. Mosor, J. Hendrickson, B. C. Richards, J. Sweet, G. Khitrova, H. M. Gibbs, T. Yoshie, A. Scherer, O. B. Shchekin, and D. G. Deppe, Appl. Phys. Lett. 87, 141105 (2005).

[51] K. Hennessy, A. Badolato, M. Wigner, D. Gerace, M. Atatüre, S. Gulde, S. Fält, E. L. Hu, and A. Imamoğlu, Nature **445**, 896 (2007).

[52] A. Muller, E. B. Flagg, P. Bianucci, X. Y. Wang, D. G. Deppe, W. Ma, J. Zhang, G. J. Salamo, M. Xiao, and C. K. Shih, Phys. Rev. Lett. **99**, 187402 (2007).

[53] D. Press, S. Gotzinger, S. Reitzenstein, C. Hofmann, A. Loffler, M. Kamp, A. Forchel, and Y. Yamamoto, Phys. Rev. Lett. **98**, 117402 (2007).

[54] J. Suffczyński, A. Dousse, K. Gauthron, A. Lemaitre, I. Sagnes, L. Lanco, J. Bloch, P. Voisin, and P. Senellart, Phys. Rev. Lett. **103**, 027401 (2009).

[55] Y. Ota, N. Kumagai, S. Ohkouchi, M. Shirane, M. Nomura, S. Ishida, S. Iwamoto, S. Yorozu, and Y. Arakawa, Appl. Phys. Exp. **2**, 122301 (2009).

[56] S. Ates, S. M. Ulrich, A. Ulhaq, S. Reitzenstein, A. Löffler, S. Höfling, A. Forchel, and P. Michler, Nature Photonics **3**, 724 (2009).

[57] A. Ulhaq, S. Ates, S. Weiler, S. M. Ulrich, S. Reitzenstein, A. Löffler, S. Höfling, L. Worschech, A. Forchel, and P. Michler, Phys. Rev. B **82**, 045307 (2010).

[58] G. Cui and M. G. Raymer, Phys. Rev. A **73**, 053807 (2006); Erratum **78**, 049904 (2008).

[59] A. Naesby, T. Suhr, P. T. Kristensen, J. Møork, Phys. Rev. A **78**, 045802 (2008).

[60] M. Yamaguchi, T. Asano, and S. Noda, Opt. Express **16**, 18067(2008).

[61] A. Auffeves, J-M. Gérard, and J-P. Poizat, Phys. Rev. A **79**, 053838 (2009).

[62] A. Auffeves, D. Gerace, J-M. Gérard, M. F. Santos, L. C. Andreani, and J-P. Poizat, Phys. Rev. B **81**, 245419 (2010).

[63] C. B. Duke and G. D. Mahan, Phys. Rev. **139**, A1965 (1965).

[64] A. V. Uskov, A.-P. Jauho, B. Tromborg, J. Mørk, and R. Lang, Phys. Rev. Lett. **85**, 1516 (2000).

[65] B. Krummheuer, V. M. Axt, and T. Kuhn, Phys. Rev. B **65**, 195313 (2002).

[66] G. Tarel and V. Sanova, Phys. Rev. B **81**, 075305 (2010).

[67] P. Kaer, T. R. Nielsen, P. Lodahl, A.-P. Jauho, and J. Mørk, Phys. Rev. Lett. **104** 157401 (2010).

[68] M. Yamaguchi, T. Asano, K. Kojima, S. Noda, Phys. Rev. B **80**, 155326 (2009).

[69] R. P. Feynman, *The Feynman Lectures on Physics*, Vol. 3 (Addison-Wesley, USA, 1965).

[70] Y. Aharonov and D. Bohm, Phys. Rev. **115**, 485 (1959).

[71] Ya. M. Blanter and M. Büttiker, Phys. Rep. **336**, 1 (2000).

[72] T. Martin, *Nanophysics : Coherence and Transport* (Les Houches, Volume Session LXXXI) eds. H. Bouchiat et. al., NATO ASI (Elsevier, Amsterdam, 2005); arXiv:cond-mat/0501208v1.

[73] A. Kumar, L. Saminadayar, D. C. Glattli,Y. Jin, and B. Etienne, Phys. Rev. Lett. **76**, 2778 (1996).

[74] M. Henny, S. Oberholzer, C. Strunk, T. Heinzel, K. Ensslin, M. Holland, C. Schönenberger, Science **284**, 296 (1999).

[75] W. D. Oliver, J. Kim, R. C. Liu, Y. Yamamoto, Science **284**, 299 (1999).

[76] P. Samuelsson, E. V. Shkhorukov, and M. Büttiker, Phys. Rev. Lett. **92**, 026805 (2004).

[77] I. Neder, N. Ofek, Y. Chung, M Heiblum, D. Mahalu, and V. Umansky, Nature **448**, 333 (2007).

[78] C. W. J. Beenakker, C. Emary, M. Kindermann, and J. Van Velsen, Phys. Rev. Lett. **91**, 147901 (2003).

[79] G. Fève, A. Mahé, J.-M. Berroir, T. Kontos, B. Plaçais, D. Glattli, A. Cavanna, B. Esienne, and Y. Jin, Science **316**, 1169 (2007).

[80] S. Ol'khovskaya, J. Splettstoesser, M. Moskalets, and M. Büttiker, Phys. Rev. Lett. **101**, 166802 (2008).

[81] J. Splettstoesser, M. Moskalets, and M. Büttiker, Phys. Rev. Lett. **103**, 076804 (2009).

[82] G. Fève, A. Mahé, J. M. Berroir, T. Kontos, B. Plaçais, D. C. Glattli, A. Cavanna, B. Etienne, and Y. Jin, Physica E **40**, 954 (2008).

[83] A. Mahé, F. D. Parmentier, G. Fève, J.-M. Berroir, T. Kontos, A. Cavanna, B. Etienne, Y. Jin, D. C. Glattli, and B. Plaçais, J. Low Temp. Phys. **153**, 339 (2008).

[84] A. Mah'e, F. D. Parmentier, E. Bocquillon, J.-M. Berroir, D. C. Glattli, T. Kontos, B. Plaçais, G. Fève, A. Cavanna, and Y. Jin, Phys. Rev. B **82**, 201309(R) (2010).

[85] Keeling, A. Shytov, and L. Levitov, Phys. Rev. Lett. **101**, 196404 (2008).

[86] M. Albert, C. Flindt, M. Büttiker, Phys. Rev. B **82**, 041407(R) (2010).

[87] T. Jonckheere, T. Stoll, J. Rech, and T. Martin, arXiv:1111.6021.

[88] G. Fève, P. Degiovanni, and Th. Jolicoeur, Phys. Rev. B **77**, 035308 (2008).

[89] P. Degiovanni, Ch. Grenier, and G. Fève, Phys. Rev. B **80**, 241307 (2009).

[90] C. Santori, D. Fattal, J. Vuckovic, G. S. Solomon, and Y. Yamamoto, Nature **419**, 594 (2002).

[91] S. Varoutsis, S. Laurent, P. Kramper, A. Lemaître, I. Sagnes, I. Robert-Philip, and I. Abram, Phys. Rev. B **72**, 041303 (2005).

[92] D. Fattal, K. Inoue, J. Vučković, C. Santori, G. S. Solomon, and Y. Yamamoto, Phys. Rev. Lett. **92**, 037903 (2004).

[93] A. Kiraz, M. Atatüre, and A. Imamoğlu, Phys. Rev. A **69**, 032305 (2004).

[94] R. Willett, J. P. Eisenstein, H. L. Störmer, D. C. Tsui, A. C. Gossard, and J. H. English, Phys. Rev. Lett. **59**, 1776 (1987).

[95] E.-A. Kim, M. Lawler, S. Vishveshwara, and E. Fradkin, Phys. Rev. Lett. **95**, 176402 (2005).

[96] S. A. Kivelson: Phys. Rev. Lett. **65** (1990) 3369.

[97] J. K. Jain, S. A. Kivelson, and D. J. Thouless: Phys. Rev. Lett. **71** (1993) 3003.

[98] C. de C. Chamon, D. E. Freed, S. A. Kivelson, S. L. Sondhi, and X. G. Wen: Phys. Rev. B **55** (1997) 2331.

[99] C. L. Kane, Phys. Rev. Lett. **90** 226802 (2003).

[100] B. Rosenow and B. I. Halperin, Phys. Rev. Lett. **98**, 106801 (2007).

[101] F. E. Camino, W. Z. Zhou, and V. J. Goldman, Phys. Rev. Lett. **98**, 076805 (2007).

[102] K. Koshino and A. Shimizu, Phys. Rep. **412**, 191 (2005).

[103] R. J. Glauber, in *Quantum Optics and Electronics*, edited by C. de Witt, A. Blandin, and C. Cohen-Tannoudji (Gordon and Breach, New York, 1965), pp. 65-185.

[104] K. Koshino, Phys. Rev. A **84**, 033824 (2011).

[105] J. Rammer and H. Smith, Rev. Mod. Phys. **58**, 323 (1986).

[106] H. Schoeller and G. Schön, Phys. Rev. B **50**, 18436 (1994).

[107] G. D. Mahan, Phys. Rev. **163**, 612 (1967).

[108] P. Nozieres and C. T. De Dominicis, Phys. Rev. **187**, 1097 (1969).

[109] K. D. Schotte and U. Schotte, Phys. Rev. **182**, 479 (1969).

[110] K. Ohtaka and Y. Tanabe, Rev. Mod. Phys. **62**, 929 (1990).

[111] K. Matveev and A. I. Larkin, **46**, 15337 (1992).

[112] I. Neder, M. Heiblum, Y. Levinson, D. Mahalu, and V. Umansky, Phys. Rev. Lett. **96**, 016804 (2006).

[113] I. Neder and F. Marquardt, New J. Phys. **9**, 112 (2007).

[114] I. Neder, M. Heiblum, D. Mahalu, and V. Umansky, Phys. Rev. Lett. **98**, 036803 (2007).

[115] I. Kulich, in *Quantum Noise in Mesoscopic Systems*, edited by Yu. V. Nazarov (Kluwer, Dordrecht, 2003); cond-mat/0209642.

[116] D. A. Abanin and L. S. Levitov, Phys. Rev. Lett. **93**, 126802 (2004).

[117] D. A. Abanin and L. S. Levitov, Phys. Rev. Lett. **94**, 186803 (2005).

[118] B. Muzykantskii, N. d'Ambrumenil, and B. Braunecker, Phys. Rev. Lett. **91**, 266602 (2011).

[119] V. Mkhitaryan and M. E. Raikh, Phys. Rev. Lett. **106**, 197003 (2011).

[120] M. Reznikov, R.de Picciotto, T. G. Friffiths, M. Heiblum, and V. Umansky, Nature **399**, 238 (1999).

[121] M. Dolev, M. Heiblum, V. Umansky,Ady Stern, and D. Mahalu, Nature **452**, 829 (2008).

[122] A. Bid, N. Ofek, M. Heiblum, V. Umansky, and D. Mahalu, Phys. Rev. Lett. **103** 236802 (2009).

[123] F. Wilczek, Phys. Rev. Lett. **48** 1144 (1982).

[124] S. B. Isakov, T. Martin, and S. Ouvry, Phys. Rev. Lett. **83**, 580 (1999).

[125] I. Safi, P. Devillard, and T. Martin, Phys. Rev. Lett. **86**, 4628 (2001).

[126] S. Vishveshwara, Phys. Rev. Lett. **91**, 196803 (2003).

[127] T. Fujii, J. Phys. Soc. Jpn. **76**, 044709 (2007).

[128] T. Fujii, J. Phys. Soc. Jpn. **79**, 044714 (2010).

[129] R. Sakano, T. Fujii, and A. Oguri, Phys. Rev. B **83**, 075440 (2011).

[130] Y. Yamauchi, K. Sekiguchi, K. Chida, T. Arakawa, S. Nakamura, K. Kobayashi, T. Ono, T. Fujii, and R. Sakano, Phys. Rev. Lett. **106** 176601 (2011).

[131] X.G. Wen, Int. J. Mod. Phys. B **6**, 1711 (1992).

[132] X.G. Wen, Int. J. Mod. Phys. B **6** (1992) 405; ibid. **44** (1995) 405.

[133] D. Ferraro, A. Braggio, M. Merlo, N. Magnoli, and M. Sassetti, Phys. Rev. Lett. **101**, 166805 (2008).

[134] M. Heiblum, Physica E **20**, 89 (2003).